Density Matrix Renormalization Group Study of the Enhanced Hole-Hopping Model of High Temperature Superconductivity

By

Bill Minor, B.Sc., M.Sc.

A Thesis Submitted to the Faculty of Graduate Studies
in Partial Fulfillment of the Requirements
for the Degree

Doctor of Philosophy

McMaster University

December 1996

DOCTOR OF PHILOSOPHY (1996) McMASTER UNIVERSITY

(Physics) Hamilton, Ontario

TITLE: Density Matrix Renormalization Group Study of the Enhanced Hole-Hopping Model of High Temperature Superconductivity

AUTHOR: Bill Minor,

B.Sc. (University of Waterloo)

M.Sc. (McMaster University)

SUPERVISOR: Dr. Frank Marsiglio

NUMBER OF PAGES: xiii, 110

Density Matrix Renormalization Group Study of the Enhanced Hole-Hopping Model of High Temperature Superconductivity

Abstract

The thermodynamic behaviour of the enhanced hole-hopping model of high temperature superconductivity is investigated using the numerical Density Renormalization Group (DMRG) technique. The enhanced hole-hopping or Δt model is a Hubbard-like lattice model that has been proposed to account for superconductivity in the high temperature superconducting materials. Extensive results for this model have been obtained by others within the BCS approximation. This thesis does not attempt to motivate the use of the Δt model but rather it is the goal of this work to characterize the accuracy of two techniques used to study this model. In particular, the ground state energy and binding energy for a pair of particles as calculated within the DMRG are compared to similar results obtained from BCS and Exact Diagonalization studies. The DMRG is a relatively new numerical technique and consequently a detailed discussion of its implementation is given. Application of the DMRG necessarily confines investigation to one dimension. Analysis of finite size effects is also presented where warranted.

Acknowledgements

Firstly I would like to thank my supervisor Frank Marsiglio for his patience, support, and guidance. I would like to thank Atomic Energy Canada Limited, Chalk River Laboratories for their hospitality and the use of their computers. I would also like to thank Dr. Jules Carbotte and Dr. John Preston for their comments and criticisms. I would like to thank the Dept. of Physics for their support.

Over the course of my stay at McMaster I have met and had discussions with many people. I would like to thank my office mates Kaori Tanaka, Dr. Julie Lefevbre, Dr. Mohamed Mansor, Yong Zhang and Dwayne Branch. I would like to thank Dave Feder for introducing me to the Lanczos routine and credit must be given to following people for answering my questions on the Density Matrix Renormalization Group: Dr. Mark Kvale, Dr. Liang Chen, and Dr. Arnold Sikkema. I would like to thank Dr. Peter Arberg for encouraging me to learn the *C* programming language and then repeatedly answering my questions about pointers. Thanks to Mark Lumsden and Peter Mason for their help with getting me started with *Linux*. I would also like to acknowledge the following people who in one way or another made an influence upon me while at MAC: Dr. Bill Atkinson, Dr. Rachid Ouyed, Hamish Johnston, Dr. Pekka Soininen,

Dr. Marcel Franz, Andy Beardsal, Rob Gojermac, Michel Bluteau, Fan Yu, and Dr. Frank Hegman. I would like to thank my partners in crime and former roomates who inspired me to study: Dr. Bruce (Jerry Ball) Takasaki, Mike (Flairgun) Varasso, Elio (Luger) Guzzo, Don (Korn Kob) Clarkner, and Ducats. Thanks also to Chat (hacksaw) Thomasson in particular for his humour and mediation skills and to Todd (Wreckin' Ball) DeSantis for the hot feet. Honourable mentions to Melissa Cole, Nancy Derhak, Zoe Simmons, lil' Lori Muldoon, Audrey LeCoarer, Shelly Kett, Lady G, Dumper, and *Duke Nukem.*

I would also like to recognize the support of the following individuals Hugh Dillon, Trent Carr, Tim White, Dale Harrison, and Steve Carr. Many thanks also to *Headstones*, Clarence Gaskel, Joe Dick, Mimi Jones, Derald Blair, The Bamford Group, Deborah Schroeder, and Dave Daniels. Thanks for everything. Hugh and Trent deserve extra recognition for reviewing the manuscript and pointing out typos.

While at McMaster one person in particular deserves extra special thanks. I have nothing to say but great things about this person. Chris Odonovan has spent many a time helping me better understand *C, Unix*, and computers in general. Without his abundant help none of this would have been possible. While his humour at times is lacking, his generosity is unsurpassed. I have enjoyed our conversations on just about everything and I will truly miss his regular company. I only hope that one day our paths may overlap once again. Chris, thanks a million!

I would like to thank my families for their support throughout the many years, Mom and Dad, little brother Bob, Terri, Jane, Wayne, Rob, neices,nephews, Inge, and Andre.

My greatest thanks to my greatest supporters throughout the entire process, Madison, Lil' One and my wife, my love, my best friend, my all, *Sara*. *Sara* many, many thanks for everything. Truly none of this would have happened without you (sorry Chris, you are secondary).

And now the Chapter is finally closed so its time to pick up a new book!

I Smile and Wave.

Contents

List of Figures

List of Tables

Chapter 1

Introduction

"... whatever we mean by what we say is not what the thing actually is, though it may be similar. For the thing is always more than what we mean and is never exhausted by our concepts." [1]

The study and subsequent attempt to explain physical processes is most often done through the medium of models. Models are a mathematical representation of simple ideas which account for the main physical features of a system. As a result, a model can often only be a modest representation of the real physical process. It is frequently the case that the model cannot be solved exactly and consequently approximation schemes must be utilized. It is then necessary to characterize how well the approximate solution reflects the exact properties of the model and in turn, whether this is an accurate portrayal of reality. The validity of a model is judged by its ability to account for currently observed behaviour and also by the integrity of its predictive capabilities. Often this hinges upon the degree to which the model must be extended in order to explain additional features. Model failures signify a design flaw or lack of

understanding and are manifest of some striking or unexpected behaviour. It is these fascinations which lend to the continual progression of understanding. The characterization of techniques used to describe a model of High Temperature Superconductivity will be the focus of this thesis.

A superconducting phase transition was first observed in 1908 when Onnes [2] reported the disappearance of resistivity in Hg when cooled to below a critical temperature T_c, of 4.2 K. A microscopic theory describing this transition was put forth in 1956 by Bardeen, Cooper, and Schrieffer (BCS) [3]. The BCS *theory* of superconductivity is a general theory of quasiparticle pairing starting from a Fermi liquid state. The BCS *model* of superconductivity further specifies that the pairing is mediated by the instantaneous exchange of phonons and that the symmetry of the superconducting order parameter is *s-wave* (zero angular momentum pairs). For the most part, the BCS model predicts universal parameter free features for many elemental and superconducting compounds which are in excellent agreement with experimental results. However slight deviations from these predictions exist and are accounted for by a more accurate generalization of BCS theory in which the electron-phonon interaction time is included. This model is referred to as Eliashberg theory [4].

Besides the solid state, the BCS theory has found remarkable success describing pairing correlations within the nucleus [5] and the physics of neutron stars. In recognition of the significance of their theory, Bardeen, Cooper, and Schrieffer were awarded the Nobel prize in physics in 1972. Before 1986, the record high T_c was about 23 K for

the compound Nb_3Ge and it was generally accepted that the highest possible critical temperature could be elevated by at most a few degrees beyond this. Superconductors of this era are now commonly referred to as *conventional* superconductors.

In 1986 Bednorz and Muller [6] made the serendipitous discovery that an appropriately doped La_2CuO_4 ceramic compound would superconduct at 30K. Moreover it has become clear that this superconductor (and others) possess features uncharacteristic of the predictions of the BCS microscopic model of superconductivity. In particular, phonons do not play a significant role in the mechanism leading to superconductivity nor does the order parameter seem to possess s-wave symmetry. To date the highest T_c is approximately 133 K for the compound $HgBa_2Ca_2Cu_3O_8$. Unconventionally natured and numbering in the hundreds, these superconductors have been labelled *High Temperature Superconductors (HTSCs)*. Whether or not, or to what degree, BCS theory may be applicable to the HTSCs remains an open question. Consequently, many models have been put forth to describe the HTSCs. The extreme relevance of Bednorz and Muller's discovery is reflected in the fact that they were awarded a Nobel prize in 1987, the shortest time ever between discovery and winning a Nobel prize. This finding has led to unprecedented furore in the physics community and yet despite intense efforts by experimentalists and theorists alike, a complete theory of HTSCs has remained elusive.

There are many proposed models of high temperature superconductivity, each with their own merits and inadequacies. For most, if not all of these models, exact solution

for realistic parameters is unavailable and some type of approximation is required. Even so, in many cases only numerical solutions are possible. The goal of this thesis is to characterize one particular model which is thought to be appropriate in describing the superconducting regime of HTSCs. By this it is meant that this thesis is not advocating the model which best governs the HTSCs, but rather the scope of this work is to assess the validity of various techniques used to study specific properties of the model in question. Study is restricted to one dimensional (1D) analysis where the likelihood for extracting exact behaviour is greatest. While 1D systems may not be very realistic the techniques utilized and conclusions reached in this thesis should prove useful for higher dimensional studies where exact solutions are not attainable.

1.1 BCS Superconductivity

Paramount to the formulation of BCS theory is the Cooper-pair problem [7] which initiated the direction in which the microscopic theory should proceed. Based on this concept, BCS intuitively determined the necessary stable ground state wavefunction in the presence of electron pairing. Subsequently, they were able to predict universal characteristics of the superconducting state which provided detailed agreement with experiments.

Cooper pointed out that the ground state of a normal metal at zero temperature is unstable. This instability is indicative of a phase transition to the superconducting state. While the demonstration of a pairing instability is not a description of the superconducting state, it is suggestive of the process by which superconductivity

occurs. Built into Cooper's pairing theory is the idea that when a pair of electrons in opposite spin and momentum states are added to a non-interacting Fermi gas, the electrons will bind together for an arbitrarily small, but attractive potential. But how could a pair of electrons overcome the repulsive Coulomb interaction and bind? What is the source of the attraction? The answer to these questions was established prior to Cooper's work. Experimentally it was observed that good conductors were poor superconductors. The reason for this became clear with the discovery of the isotope effect by Maxwell [8] and Reynolds et al. [9] These groups found that T_c was strongly dependent on the mass of the constituent isotopes, M. In particular, for tin and thallium the following relation was formulated

$$T_c \propto M^{\frac{-1}{2}}.$$

These experiments clearly indicated that the lattice was somehow responsible for superconductivity. Frohlich [10] further studied the interactions of electrons in a metal with acoustic lattice vibrations (phonons). He demonstrated that phonons could mediate an attractive interaction between electrons at the Fermi surface. Phonon effects could be included in an indirect manner in an instantaneous effective electron-electron interaction

$$V_{\vec{k},\vec{k}'} = \frac{2|g_{\vec{k}-\vec{k}'}|^2\hbar\omega_{\vec{k}-\vec{k}'}}{(\epsilon_k - \epsilon_{k'})^2 - \omega^2_{\vec{k}-\vec{k}'}}$$

where $g_{\vec{k}-\vec{k}'}$ is the amplitude for an electron being scattered by a phonon and $\omega_{\vec{k}-\vec{k}'}$

is the phonon dispersion. This potential is attractive for $|\epsilon_k - \epsilon_{k'}| < \hbar\omega_{\vec{k}-\vec{k}'}$. Thus the electron-phonon scattering which limits conductivity in the normal state can also provide an attractive potential necessary for binding. Physically the attraction can be pictured as resulting from the first electron polarizing the ionic crystal field around it, which in turn serves as an enhanced positive field to which a second electron is attracted. Cooper replaced the overall potential with a model interaction of the form

$$\begin{aligned} V_{\vec{k},\vec{k}'} &= -V \qquad \text{for } |\epsilon_{\vec{k}}|, |\epsilon_{\vec{k}'}| < \omega_D \\ &= O \qquad \text{otherwise} \end{aligned} \tag{1.1}$$

where ω_D is the Debye frequency which characterizes the energy of the phonons exchanged in the scattering process. Scattering events in conventional superconductors are essentially confined to the Fermi surface as $\omega_D \sim 10meV$ while the Fermi energy is of order $10eV$.

Assuming the two electrons are in a spin singlet state a ground state trial wavefunction can be taken as

$$|\psi\rangle = \sum_k \alpha(k) c^\dagger_{k,\uparrow} c^\dagger_{-k,\downarrow} |F\rangle$$

where $|F\rangle$ represents the filled Fermi sea and $c^\dagger_{k,\uparrow}$ creates an electron in momentum state k with spin-up. For $|\psi\rangle$ to be normalized the coefficients $\alpha(k)$ must satisfy the condition

$$\sum_k |\alpha(k)|^2 = 1.$$

Using the above model potential, wavefunction, and normalization, minimization of the energy within a variational approach, shows that two electrons bind with an energy

$$E = -2\hbar\omega_D e^{\frac{-2}{N(0)V}}$$

where $N(0)$ is the density of states at the Fermi surface. [1]

In the many-body (pair) case, BCS assumed the pairs had zero center-of-mass momentum and that the appropriate many-body Hamiltonian had the following *reduced* form

$$H_{red} = \sum_{k,\sigma} \epsilon_k c^\dagger_{k,\sigma} c_{k,\sigma} + \frac{1}{N} \sum_{k,k'} V_{k,k'} c^\dagger_{k,\uparrow} c^\dagger_{-k,\downarrow} c_{-k',\downarrow} c_{k',\uparrow}$$

where ϵ_k is the single particle energy and $V_{k,k'}$ is the two body potential. The derivation of such a many-body Hamiltonian will be elaborated on later in Chapter 2. BCS proposed that the ground state wavefunction of a superconducting system is given by

$$|\psi\rangle = \prod_k [u_k + v_k c^\dagger_{k,\uparrow} c^\dagger_{-k,\downarrow}|0\rangle$$

[1] One could have taken a trial wavefunction with the spins in the triplet state, however no non-trivial solution exists for the energy. See [11]

where $|0\rangle$ is the vacuum state and the coefficients u_k and v_k indicate the probability amplitude for a state k being unoccupied or occupied by a pair, respectively. It is interesting to note that unlike the Cooper pair wavefunction, the BCS wavefunction does not conserve particle number but rather contains a mixture of states with $0, 2, 4, 6, \ldots, N-2, N, N+2, \ldots$ particles. This violation of particle conservation is handled by working in the grand canonical ensemble and invoking the condition that only the average number of particles be equal to the actual number of particles in the system. The statistical fluctuation in particle number is then of order $N^{\frac{1}{2}}$ which when compared to N for macroscopic systems is insignificant.

Invoking the variational principle u_k and v_k can be determined by minimizing the energy. The results are [12]

$$\begin{aligned} u_k^2 &= \frac{1}{2}[1 - \frac{\epsilon_k}{E_k}] \\ v_k^2 &= \frac{1}{2}[1 + \frac{\epsilon_k}{E_k}] \\ u_k^2 + v_k^2 &= 1 \end{aligned} \tag{1.2}$$

where the normal state dispersion ϵ_k for an electron gas with chemical potential μ is

$$\epsilon_k = \frac{\hbar^2 k^2}{2m} - \mu$$

with the excitation spectrum in the superconducting state given by

$$E_k = \sqrt{\epsilon_k^2 + \Delta_k^2}.$$

Δ_k is the superconducting order parameter or gap in the quasiparticle spectrum and it signifies the minimum excitation energy required to break up a quasiparticle pair. The solution for Δ_k is given by the non-linear integral equation

$$\Delta_k = \frac{-1}{N} \sum_{k'} V_{k,k'} \frac{\Delta_{k'}}{2E_{k'}}$$

while the chemical potential must be determined self-consistently from

$$n = 1 - \frac{1}{N} \sum_{k} \frac{\epsilon_k}{E_k}$$

where n is the density of particles.

It should be pointed out that the condensation energy of the superconducting state is of the order of meV while the correlation energies in a metal are typically in eV range. It is remarkable that BCS were able to isolate the interaction responsible for pairing considering the disparity between energy scales involved. This is reconciled by the fact that the pairing is between Landau quasiparticles rather than bare electrons. Within Fermi liquid theory [13] the large correlation energy is folded into the renormalized mass of the quasiparticles so that in actuality, superconductivity occurs due to the weak attraction of long-lived quasiparticles.

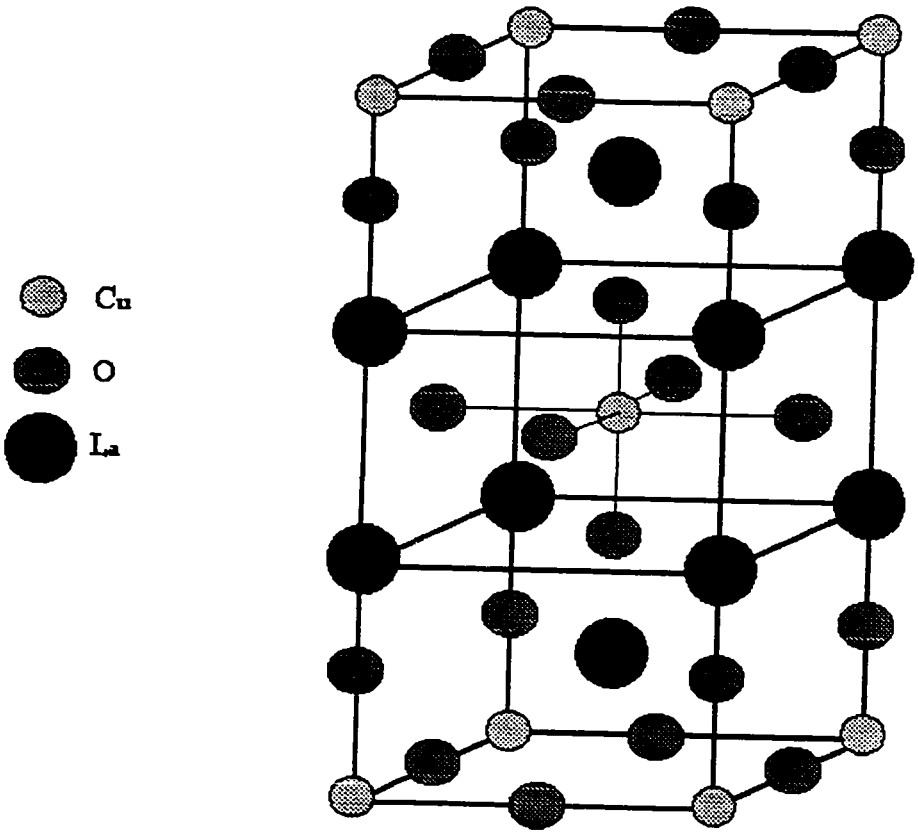

Figure 1.1: Crystal Unit Cell for HTSC Lanthanum Copper Oxide

1.2 Overview of High Temperature Superconductors (HTSCs)

High temperature superconductors possess properties markedly different from conventional BCS superconductors such as aluminum (Al). As such the application of BCS theory to explain high temperature superconductivity is questionable. HTSC compounds are formed from complex crystal structures which reflect their multi-atom unit cells. The crystal anisotropy in these materials is the basis for their striking

characteristics. Figure 1.1 illustrates the unit cell for the HTSC parent compound lanthanum copper oxide (La_2CuO_4) or *214*. When optimally doped with strontium to form $La_{1.85}Sr_{0.15}CuO_4$, this compound becomes superconducting at a transition temperature (T_c) of about 35 K. The crystal structure contains two copper oxide planes per unit cell. It is these planes where conduction is thought to take place in the HTSCs with the surrounding structure functioning as a charge reservoir. There exists a large number of HTSC variants but all do *not* seem to have copper-oxygen planes in common. For example the compound $Ba_{1-x}K_xBiO_4$ with a $T_c \approx 30K$ does not possess copper-oxide planes and is almost isotropic. Consequently the term *oxides* is occasionally used to refer to high temperature superconductors.

A simple, yet extremely rich, phase diagram for the properties of the HTSC compound 214 as a function of temperature and Sr doping is shown in Figure 1.2. HTSC cuprates in general posess the same attributes depicted by this phase diagram. At zero doping ($x = 0$) there is an antiferromagnetic insulating state which disappears quickly upon substitution with a small amount of dopant. If the temperature is low enough, the transition is to the superconducting phase otherwise it is to a metallic state. The metal-insulator phase change is known as the *Mott* transition.

Various experiments such as flux quantization confirm that the carrier charge in the superconducting state in these compounds is twice that of the electron charge. Additionally, measurement of the sign of the Hall coefficent indicates that holes are being doped into the system. Superconductivity is attained with a T_c which at first

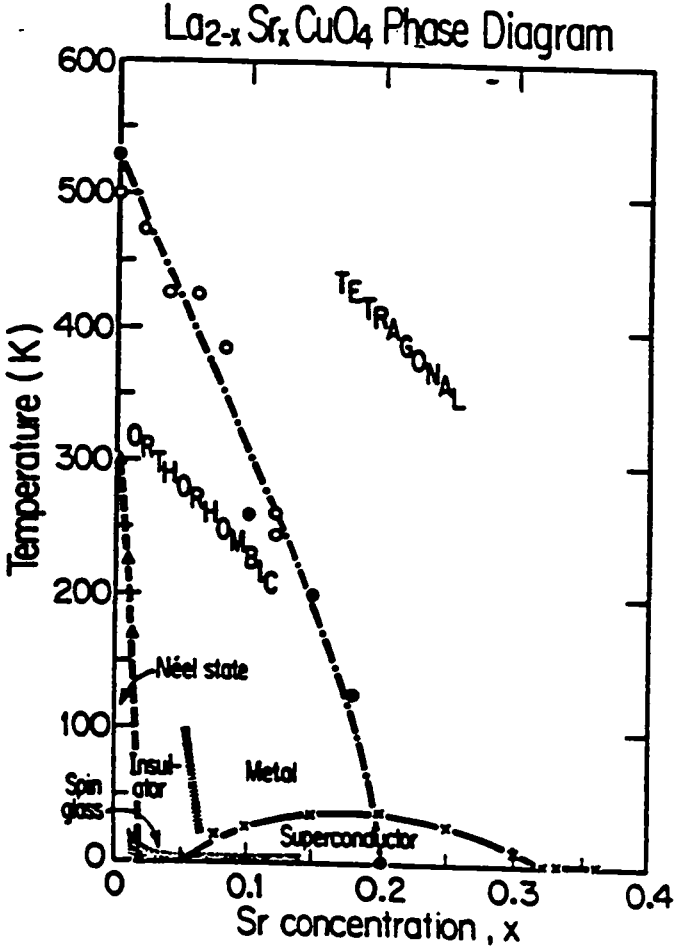

Figure 1.2: Phase Diagram for the HTSC Lanthanum Copper Oxide

increases (*underdoped regime*), reaches a maximum and then decreases as doping increases (*overdoped regime*). The hole doping at which the maximum T_c is reached is known as *optimal doping*. As the superconducting phase vanishes with increased doping, free electron behaviour sets in and the normal metal phase is established. This is to be contrasted with a *localized* metallic phase which results from doping the insulating state at temperatures too high to produce superconductivity. Besides electronic phases, there is also a structural transition where the material transforms

from an orthorhombic crystal structure to a tetragonal one. This structural distortion can be viewed in terms of the tilting of oxygen octahedra which are formed from the apical oxygen ions on either side of the CuO_2 planes. The generic phase diagram just described classifies the HTSCs known as *hole-doped* superconductors. There also exists a class of HTSCs referred to as *electron-doped* cuprates, a typical example being the compound $Nd_{2-x}Ce_xCuO_4$. However, the sign of the Hall coefficient in the electron doped materials and its correlation to carrier charge is not as precise as it is for the hole case [14]. The phase diagram for the electron-doped compounds contains the same generic features as the hole-doped cuprates with a few subtle differences. The insulating state in the electron case does not disappear as quickly with doping as in the hole case and the transition to the superconducting state is much sharper. Another discrepancy not portrayed by the phase diagrams is the symmetry of the order parameter. Electron-doped HTSCs seem to be capably described by a BCS-type order parameter whereas it appears that the hole doped materials do not have s-wave order. In particular, photoemission measurements [15] suggest a large degree of gap anisotropy with the gap actually going to zero (gap nodes) at several points on the Fermi surface. Tunneling experiments have been performed [16] which can probe the symmetry of the gap or pair wavefunction. These measurements suggest that the superconducting pairs are of *d-wave* $x^2 - y^2$ symmetry. This symmetry is consistent with gap nodes on the Fermi surface. The fact that both cuprates apparently have different order parameters is suggestive of two possible pairing mechanisms, troublesome

concept for some theorists to accept.

By examining the electronic structure of the HTSCs light can be shed on some aspects of the phase diagram. Analysis will be with regards to the hole doped cuprates using the lanthanum compound as the archetype. As the copper-oxide planes are responsible for conduction discussion is restricted to their role. Naïve electron counting suggests the valence states for the constituents in the 214 parent compound are O^{2-}, La^{3+}, and Cu^{2+}. Thus the Cu^{2+} ion has a partially filled degenerate $3d$ electron shell with a single hole. The six oxygen electrons also form a degenerate level of $2p$ character and lower in energy than the copper level. In the presence of crystal field splitting (Jahn-Teller effect) these degeneracies are lifted to leave a half-filled Cu level of $3d_{x^2-y^2}$ character with all other states filled. In the absence of electron interactions the 214 compound would be classified as a metal according to coventional band theory arguments. However, as indicated on the phase diagram it is actually an antiferromagnetic insulator. To place another electron in the Cu shell would cost an additional Coulomb energy of about $10eV$ and it is this localization of copper moments that gives rise to the observed magnetic effects. Consequently, in the HTSCs *strong correlations* must be taken into account, that is the average interaction energy significantly exceeds the average kinetic energy. The existence of strong interactions contradicts the requirements of Landau's Fermi liquid theory where the effect of weak interactions is folded into a renormalized mass. Upon doping 214, as Sr prefers to be in a 2+ ionic state, each ionic substitution of La donates a hole carrier to the

CuO_2 planes. Electronic motion then arises from hopping between weakly correlated oxygen p-orbitals.

In conventional superconductors the electron-phonon mechanism manifests itself in an observed isotope effect. Most elemental superconductors have only one atom per primitive cell and within the Debye model the phonon frequency is inversely proportional to the ionic mass. With the HTSC compounds having many atoms per primitive cell the phonon modes are much more complicated. Nevertheless the lack of a definitive isotope effect seems to rule out phonon-mediated pairing.

As previously mentioned BCS theory is constructed within a Fermi liquid paradigm. Fermi liquid theory predicts the temperature dependence of the electrical resistivity in the normal state. By examining scattering events at the Fermi surface simple arguments [17] dictate that the scattering rate of quasiparticles or the resistivity goes as $(k_B T)^2$ where k_B is the Boltzmann constant. The normal state temperature dependence of the resistivity in the copper oxide planes of the HTSCs is *linear* over a large temperature range. The implications of this are that Fermi liquid theory demands that excitations close to the Fermi surface must be sufficiently long lived that the quasiparticles are well defined near the Fermi energy. That is, the scattering or damping rate must be small. This suggests that Landau's theory is valid for energy scales much smaller than the Fermi energy or that the theory is applicable only in the zero temperature limit. Since resistivity varies linearly with T in the HTSCs, the average decay width of the low lying excitations is comparable to their average

energy. This feature raises serious doubts about the application of Fermi liquid and hence BCS theory, to the HTSCs, particularly in the underdoped regime [18].

The foregoing overview serves to illustrate the unusual behaviour of the high-T_c oxides and the key features of these compounds which must be accounted for in a proposed model. It is widely believed by many that to properly account for these materials electronic correlations must be taken into account with greater detail.

1.3 Overview

There is strong evidence that HTSCs do not conform to the conventional model of superconductivity as put forth by BCS. In particular, it is apparent that attempts to theoretically model the HTSCs must take strong correlations into account. In Chapter 2 theoretical models used to study electronic correlations will be presented. Many-body problems are inherently difficult to solve exactly and consequently exact study is often restricted to one-dimensional systems where the mathematics and numerics is tractable. In Chapter 3 model results will be presented within Exact Diagonalization studies and contrasted to related investigations. The Density Matrix Renormalization Group will be the focus of Chapter 4. This numerical technique will be reviewed in detail and then applied to the theoretical models under study. The results of this approach will be compared to the observations of Chapter 3. Finally, Chapter 5 will give the conclusions of this work.

Chapter 2

Theoretical Models

2.1 Correlation

The characteristic effects of electronic correlations can be appreciated by studying small systems such as molecules. In particular, correlations were studied with regards to chemical bonding in the hydrogen molecule H_2 by two distinct processes. Heitler and London [19] proposed a ground state wavefunction for H_2 whereby the two electrons are strongly correlated. Specifically, the ground state is a singlet of the form

$$\psi_{HL}(\vec{r_1},\vec{r_2}) = \frac{1}{2}[\phi_1(\vec{r_1})\phi_2(\vec{r_2}) + \phi_2(\vec{r_1})\phi_1(\vec{r_2})](\alpha_1\beta_2 - \beta_1\alpha_2), \tag{2.1}$$

where $\phi_1(\vec{r})$ and $\phi_2(\vec{r})$ are centered on atoms 1 and 2 and the spinors α and β represent spin up and spin down, respectively. The ionic configurations $\phi_1(\vec{r_1})\phi_1(\vec{r_2})$ and $\phi_2(\vec{r_1})\phi_2(\vec{r_2})$ are excluded so that the two electrons stay completely away from one another. In the limit of small atomic separation, however, this wavefunction does

not reduce to the proper limit, that being the wavefunction of a helium atom. Conversely, Hartree, Fock and Slater [20] presented a different approach to this problem. They regarded the electrons as being independent of one another but experiencing an average self-consistent field generated by the other $N-1$ electrons. Within this approximation the ground state wavefunction is given by

$$\psi_{HF}(\vec{r_1},\vec{r_2}) = \frac{1}{2}[\phi_1(\vec{r_1})\phi_1(\vec{r_2})+\phi_1(\vec{r_1})\phi_2(\vec{r_2})+\phi_2(\vec{r_1})\phi_1(\vec{r_2})+\phi_2(\vec{r_1})\phi_2(\vec{r_2})](\alpha_1\beta_2-\beta_1\alpha_2). \tag{2.2}$$

In this case the ionic states enter with equal weight compared to the non-ionic ones. When two hydrogen atoms are pulled apart, this wavefunction does not reduce to the proper atomic description of two separate H atoms. In fact the true ground state wavefunction of the H_2 system lies somewhere between these two extremes. These arguments are general and apply to the description of the solid state as well. The spatial extent of the valence electronic wavefunction R is large and comparable to the separation between lattice sites d, so that the electrons are essentially free and have a large dispersion or bandwidth. In the opposite extreme where $R << d$, there is very little dispersion (narrow bandwidth) and the electrons are best described by atomic-like states. The former case where correlations are weak corresponds to the metallic state wheres in the latter case very strong electronic interactions prevent charge fluctuations and the solid is an insulator. A model which attempts to account for both extremes as well as the more difficult intermediate crossover region, is known

as the Hubbard model [21].

2.2 The Hubbard Model

The Hubbard model represents one of the simplest models which can be used to describe interacting fermions on a lattice. This model was proposed by Hubbard in 1963 in order to study the approximate behaviour of electronic correlations in narrow energy bands. Simply stated, the Hubbard model expresses the competition between the repulsive Coulomb interaction and the kinetic energy or single particle hopping from site to site.

In general the Hamiltonian for a group of N particles interacting on a lattice can be written in second quantized notation as,

$$H = -\sum_{i,j,\sigma}(t_{i,j}c^{\dagger}_{i,\sigma}c_{j,\sigma} + h.c.) + 1/2\sum_{i,j,k,l}\sum_{\sigma,\sigma'}\langle ij|V^{Coul.}|lk\rangle c^{\dagger}_{i,\sigma}c^{\dagger}_{j,\sigma'}c_{l,\sigma'}c_{k,\sigma} \tag{2.3}$$

where $c^{\dagger}_{i,\sigma}(c_{i,\sigma})$ creates (annihilates) a fermion at site i with spin $\sigma(\sigma = \uparrow \; or \; \downarrow)$ and where

$$t_{i,j} = t(\vec{R}_i - \vec{R}_j) = -\int d\vec{r}\Phi^*_i(\vec{r})(\frac{\hbar^2}{2m}\vec{\nabla}_r)\Phi_j(\vec{r}) = t^*_{j,i} \tag{2.4}$$

$$\langle ij|V|kl\rangle = \int d\vec{r}d\vec{r'}\Phi^*_i(\vec{r})\Phi^*_j(\vec{r'})V(\vec{r}-\vec{r'})\Phi_k(\vec{r'})\Phi_l(\vec{r}) \tag{2.5}$$

$\Phi_i(\vec{r})$ represents the Wannier function for the i^{th} lattice site with lattice vector $\vec{r}$. Equation (2.4) is usually referred to as the *overlap* integral which specifies the hopping amplitude from site i to j while (2.5) is just the spin-independent Coulomb matrix element.

Equation (2.3) can yet be simplified further and still retain the essential physics of strongly correlated fermions. Within the tight-binding model, $t_{i,j}$ decays fairly rapidly with distance so that the hopping occurs only between nearest-neighbour (n.n.) sites with a constant amplitude i.e.,

$$\begin{aligned} t_{i,j} &= t \qquad \text{if i,j are n.n.,} \\ &= 0 \qquad \text{otherwise.} \end{aligned} \tag{2.6}$$

Furthermore, the electron-electron Coulomb interaction is taken to be effectively screened when the particles are far apart. Hubbard assumed that the dominant Coulomb contribution results when $i = j = k = l$, that is when two fermions of opposite spin occupy the same lattice site. The resulting model Hamiltonian

$$H = -t \sum_{\langle i,j \rangle, \sigma} (c^{\dagger}_{i,\sigma} c_{j,\sigma} + h.c.) + U \sum_{i} n_{i,\uparrow} n_{i,\downarrow} \tag{2.7}$$

is known as the one-band Hubbard model in the tight-binding approximation. The sums run over lattice sites with $\langle i, j \rangle$ denoting a sum over nearest neighbour sites and

the number operator $\hat{n}_{i,\sigma} = c^{\dagger}_{i,\sigma} c_{i,\sigma}$ just counts whether or not a site is occupied. The Hilbert space of this system is a tensor product of only four states per site $|0\rangle$, the vacuum, $|\uparrow\rangle$ a single spin up particle, $|\downarrow\rangle$ a single down spin particle and $|\uparrow\downarrow\rangle$ an up-down pair. This Hamiltonian can be written in k-space by Fourier transforming Equation 2.7 to

$$H = \sum_{k,\sigma} \epsilon_k c^{\dagger}_{k,\sigma} c_{k,\sigma} + \frac{U}{N} \sum_{k',k,q} c^{\dagger}_{k,\uparrow} c^{\dagger}_{-k+q,\downarrow} c_{-k'+q,\downarrow} c_{k',\uparrow} \tag{2.8}$$

where the band energies are given by

$$\epsilon_k = -2t \sum_{\delta} cosk \cdot \delta \tag{2.9}$$

with δ summing over the coordinates. It can be verified that Equation 2.7 is electron-hole symmetric by making an electron-hole transformation assuming a bipartite lattice structure [27, 28].

The Hamiltonian discussed thus far is actually referred to as the *single-band* Hubbard model. A schematic band structure for this model is shown in the top diagram of Figure 2.1. In this diagram there is a *lower* Hubbard band (LHB) and an *upper* Hubbard band (UHB) separated from one another by an energy gap (*Mott-Hubbard gap*) of magnitude U. Half-filling corresponds to the situation where there is one particle on each site so that the LHB is completely filled while the UHB is empty. To

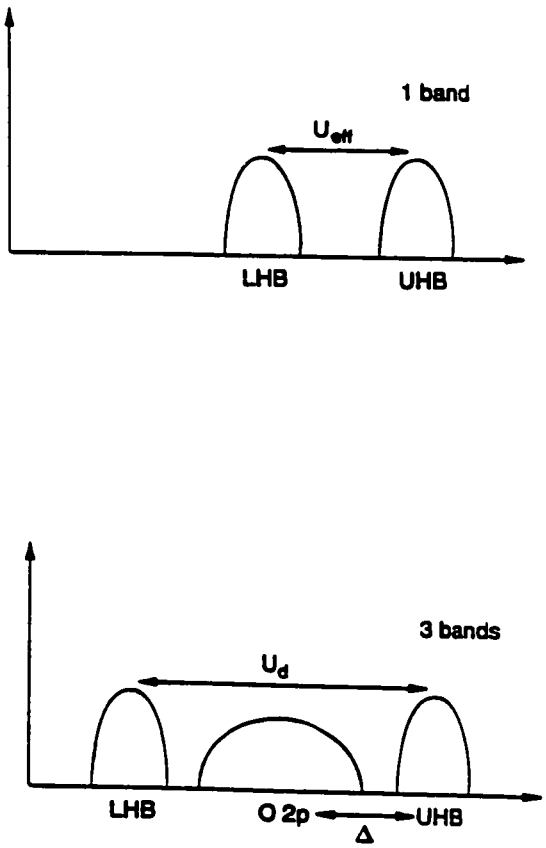

Figure 2.1: Schematic Band Structure Diagrams for the Hubbard Model.

add an extra particle at this filling, one lattice site would become doubly occupied and this cost in energy forces the particle to reside in the UHB. For particle occupations less than half-filling the valence state lies in the LHB. In this case there is no gap to the single particle excitations and this scenario corresponds to the metallic state whereas at half-filling the gap in the spectrum signifies the insulating state. In the HTSCs it is widely believed that the electronic behaviour in the copper-oxide planes is best described by a *3-band* Hubbard model. The copper-oxide unit cell is shown

in Figure 2.2 and the three bands referred to are the Cu $d_{x^2-y^2}$ orbital and two O $2p_\sigma$ orbitals. The corresponding density of states is shown in the bottom diagram of Figure 2.1. The band structure has an upper and lower Hubbard band similar to the one band case but lying between the two is a separate band. In the HTSCs the UHB and LHB are associated with the copper orbital while the band in between arises from the oxygen orbitals. In the parent HTSC compounds the copper band is half-filled while the oxygen band is completely filled. The gap of about $1.5 - 2.0eV$ between the filled O band and the empty copper UHB is commonly called the *charge-transfer* gap [1]. In this model holes are doped into a *full* oxygen band whereas electrons would be doped into a half-filled copper band. It has been shown [22] that the 3-band Hubbard model can be reduced to a one-band Hubbard model with a coupling that approximately reproduces the spectrum of the more involved Hamiltonian. This is accomplished by *folding* the O orbitals in the 3-band model into the copper orbitals so as to produce a single-band model which mimics the charge-transfer gap with an effective value of the Hubbard Coulomb repulsion U_{eff}. Unlike the 3-band model, doping in the single-band model for *both* holes and electrons is with respect to a half-filled band. There are those [23] that believe that the physics of the HTSC planes can be properly achieved with only the 3-band model.

As previously stated the Hubbard model is the simplest model one can utilize to study electronic correlations in a solid. However, the physics of such a model is extremely

[1] This charge-transfer gap is not related to the gap of the same name defined in Chapter. 3. The latter is defined as the energy required to break up a pair of bound particles.

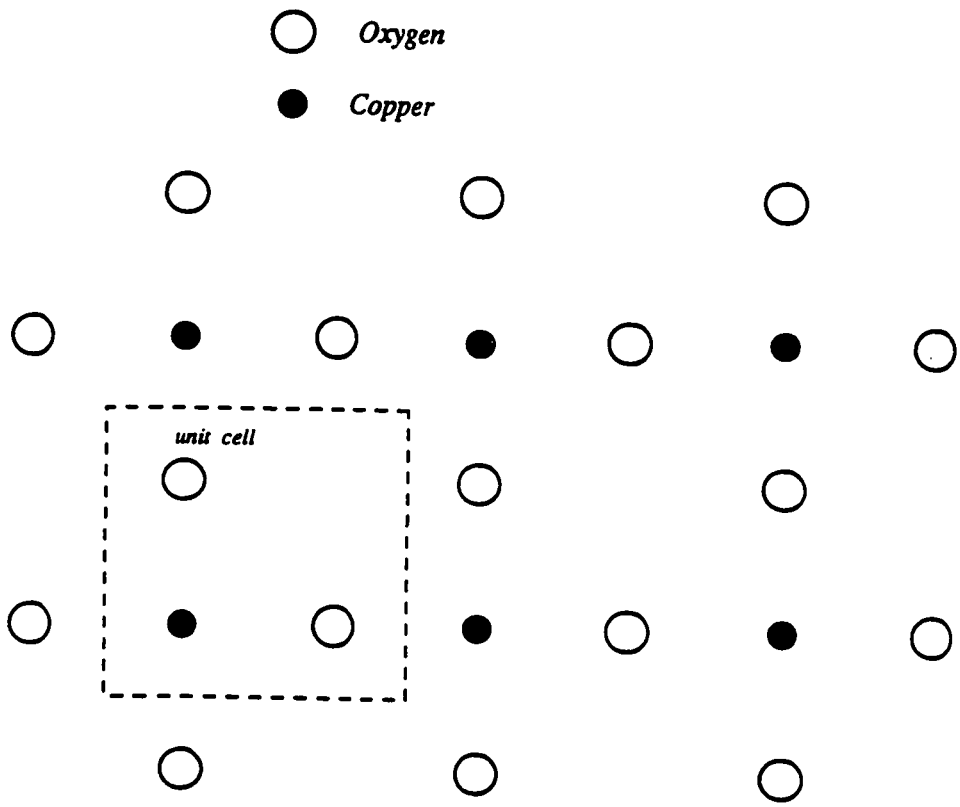

Figure 2.2: The Unit Cell for the Copper-Oxide Planes in the HTSCs.

rich and at times, subtle. In fact an exact solution for the Hubbard model exists in only $1D$ [24] and infinite [25] dimensions and even here the physics is not easy to extract. The $1D$ Hubbard model will be discussed in further detail in the next Section. A complete understanding of this model in $2D$ and $3D$ is still lacking despite years of intense study. Useful physics has been obtained with this model in certain limits utilizing various approximation schemes. In particular, the behaviour appears to be well understood at half-filling in the $U = 0$ case and the large U coupling regime.

In the weak coupling case, the interaction represents a weak perturbation on an otherwise free fermion system. In the strong coupling range and at half-filling, it costs too much energy for a particle to hop onto an occupied site. Using second order perturbation theory it can be shown [28] that the half-filled strong coupling Hubbard Hamiltonian maps onto the spin-$\frac{1}{2}$ Heisenberg antiferromagnet. It is this insulating phase which makes the Hubbard model a particularly attractive paradigm for discussing microscopic theories of HTSCs. Just away from half-filling the kinetic energy term will permit charge motion and the effective Hamiltonian now has the form of the *t-J model* [26]. The t-J model corresponds to the strong coupling limit of the Hubbard model where double site occupancy is forbidden.

Despite intense efforts, no consensus on the existence of superconductivity in the Hubbard model has yet been reached.

2.3 $1D$ Hubbard Model

In this thesis properties of the $1D$ Hubbard and $1D$ Hubbard-like models are to be studied. One dimensional Hamiltonians are worthy of study since the mathematics and numerics are more manageable than in higher dimensions thereby increasing the potential for finding an exact solution. However, it is often not known to what degree $1D$ results may be carried over to higher dimension. In reality no system is one-dimensional but in some cases because interactions are dominant only in one direction, the system can be effectively modelled in $1D$. As previously mentioned

the $2D$ and $3D$ Hubbard models are far too complex to be solved exactly. In $1D$ an exact solution has been found [24] utilizing the Bethe Ansatz [29]. The exact energies of the ground state and all the excited states are given in terms of the solution of a system of coupled nonlinear equations. The drawback to this solution is that the corresponding wavefunctions have an extremely complex form making the explicit calculation of matrix elements, correlation functions and other physical quantities very difficult. The conditions for integrability using the Bethe Ansatz technique are very restrictive so that only a small class of models, such as the $1D$ repulsive and attractive Hubbard models, can be solved with it. For $1D$ models in which an exact solution is lacking, a new numerical technique has been developed which allows for the examination of the thermodynamic limit. This technique will be used in Chapter 4 to test approximations made for models where the Bethe Ansatz cannot be applied. The development, application, and results of this technique form the crux of this dissertation.

The Bethe Ansatz was first formulated by Bethe to solve the Heisenberg spin chain system. Many years later Lieb and Wu [24] successfully applied the technique to the $1D$ Hubbard model. By no means will the technique be outlined here as it is rather involved and there are many references on the topic [30]. Rather an overview of the results for the $1D$ Hubbard model will be presented. Lieb and Wu were able to obtain the following analytic expression for the ground state energy per particle at half-filling

$$\frac{E_o}{N} = -4|t| \int_0^\infty dx \, \frac{J_0(x)J_1(x)}{x[1 + exp(\frac{xU}{2|t|})]} \tag{2.10}$$

where the $J_\nu(x)$ are Bessel functions. Their work also revealed that in the half-filled ground state (one electron per lattice site) there is a *Mott-Hubbard* or *metal-to-insulator* transition. That is, for all values of $U > 0$ the ground state is insulating and is necessarily antiferromagnetic as dictated by a theorem due to Lieb and Mattis [31] which states that in $1D$ systems the total spin in the ground state must be zero. As an aside, it should be pointed out that Landau and Lifshitz's [32] proof that long range order (LRO) cannot exist in $1D$ systems holds only for finite temperatures, while the ground state is another matter.

Numerical results for the ground state energy as a function of density and U were later provided by Shiba [33]. Shiba presented useful analytical expressions for the ground state energy as a function of density for certain values of the coupling $|U|/t$. They are

$$\begin{aligned} \frac{E_o}{tN_a} &= \frac{-4}{\pi} sin(\frac{1}{2}\pi\frac{N}{N_a}) \qquad \text{for U=0,} \\ &= -[\frac{2}{\pi} sin(\pi\frac{N}{N_a}) + t\frac{4ln2}{U}(\frac{N}{N_a})^2[1 - \frac{sin(2\pi\frac{N}{N_a})}{2\pi\frac{N}{N_a}}] \qquad \text{for U>>t,} \end{aligned} \tag{2.11}$$

where the density n is given by the total number of particles N over the total number of lattice sites N_a. For $|U|/t \rightarrow \infty$ the expression reduces to

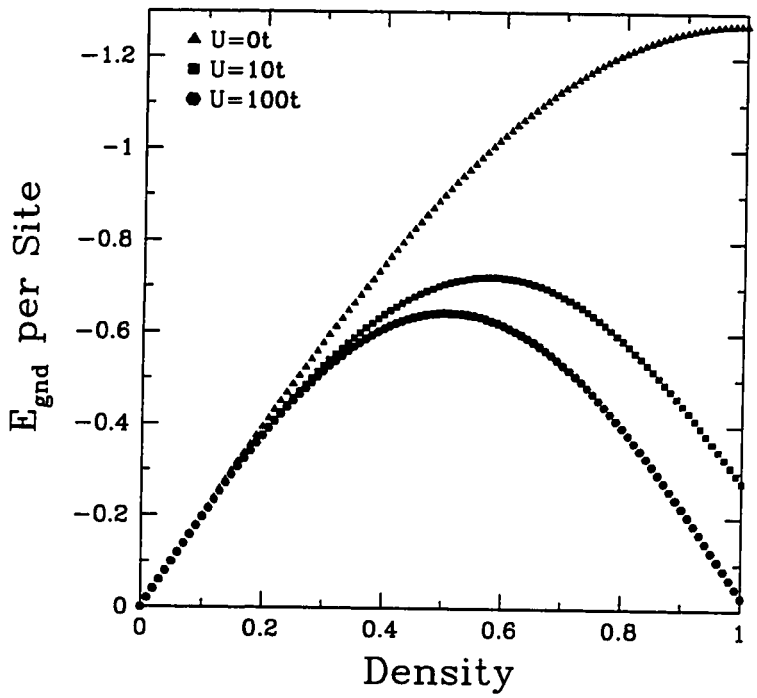

Figure 2.3: The Ground State Energy vs. Density for Various Coupling Strengths

$$\frac{E_o}{tN_a} = \frac{-2}{\pi} sin(\pi \frac{N}{N_a}) \tag{2.12}$$

and in the case of half-filling $n = (\frac{N}{N_a}) = 1$, this expression also reduces to the ground state energy of the $1D$ Heisenberg antiferromagnet with the exchange coupling constant $J = \frac{2t^2}{U}$.

In Figure 2.3 the ground state energy is plotted against number density for couplings

of $U/t = 0$, 10.0, and 100 using Equation 2.11. This plot illustrates some of the features of electron correlation. At low density the effect of correlation on the ground state energy is not significant as the three curves follow one another closely. In the low density or dilute limit, the electrons can avoid each other without compromising their kinetic energies. For non-interacting electrons in $1D$ the dispersion relation is simply

$$\epsilon_k = -2tcosk_x, \tag{2.13}$$

where k_x is the $1D$ momentum, so that the density of states $N(\epsilon)$ or the number of states between dk and $k + dk$ is

$$\begin{aligned} N(\epsilon)d\epsilon &= \frac{2}{2\pi}dk \\ N(\epsilon) &= \frac{1}{\pi}(\frac{d\epsilon}{dk})^{-1} \\ &= \frac{1}{2t\pi}\frac{1}{\sqrt{1-(\frac{\epsilon}{2t})^2}}. \end{aligned} \tag{2.14}$$

This $1D$ density of states is plotted in Figure 2.4. This plot illustrates the fact that in the dilute limit because electrons occupy the bottom of the band (energies close to $-2t$) there is a high density of states.

It can be seen in Figure 2.3 that as the density increases correlation effects set in and are most dominant at half-filling. In this case correlations prevent charge fluctuations

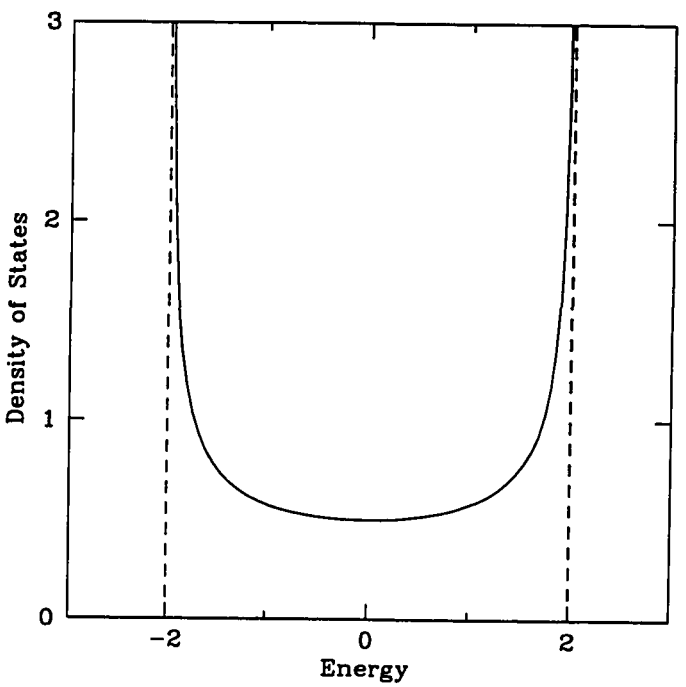

Figure 2.4: The $1D$ Density of States.

necessary for conduction and the insulating state sets in. Also of note is that as $|U|/t$ increases the minimum in the ground state energy shifts away from half-filling. This conveys the fact that the system can only gain (kinetic) energy through hopping processes involving vacant sites, so that the minimum shifts as U increases.

2.4 Spin-Charge Separation

As previously mentioned one of the motivations for studying $1D$ systems is to elucidate characteristics that may be generalized to higher dimension. In particular, in the case of the Hubbard model there are unsettled raging debates over the existence of quasiparticles in the $2D$ system. There are basically two schools of thought in this scenario, one principally founded and backed by Philip Anderson [34], which is commonly called exotic, and stems from results obtained in $1D$. The other camp, which includes many backers, takes a conventional point of view, that $2D$ systems, like $3D$ systems, are Fermi liquid based with well-defined quasiparticles. While this controversy is beyond the scope of this thesis, it is nonetheless an extremely interesting problem which illustrates radical new concepts and serves to demonstrate the discretion required in generalizing a model's characteristics. It is well established that a $1D$ interacting Hubbard system is not a Fermi liquid, that is, there are no quasiparticle-like excitations. In fact, in the vicinity of the Fermi level the momentum distribution does not show a finite discontinuity characteristic of a Fermi liquid system. In Fermi liquid theory a step-like discontinuity in the momentum distribution implies the existence of well-defined quasiparticles. In this case there is no discontinuity at the Fermi level. Behaviour of this type is associated with a *Luttinger liquid* in which there are collective low energy excitations with a separation of the spin and charge degrees of freedom. The spin excitations which do not posess charge, are called *spinons*, while the name *holons* has been given to the excitations which are endowed with charge but

lack spin. The $1D$ repulsive Hubbard model is a Luttinger liquid while the attractive Hubbard model is not.

2.5 Δt Model

It has been argued [35] that the one-band Hubbard model is incapable of properly describing the physics of high temperature superconductors. Moreover, recent experiments [36] find a doping asymmetry between electron and hole HTSCs in accord with electronic structure models based on the 3-band rather than the single-band Hubbard model. Hirsch [37] argues that the reason for this is that the one-band Hubbard model assumes two electrons on a doubly occupied site share the same atomic orbital. This is incorrect as the intra-atomic Coulomb repulsion between electrons is larger than the spacing of atomic energy levels. First principles calculations [38] of the energetics of H^- system support this view. If both electrons occupy the $1s$ orbital they would experience a repulsion of $17eV$ and the total atomic energy would be $-10.20eV$. If however, the second electron was to occupy the $2s$ level its energy would be $10.20eV$ above the $1s$ orbital. The repulsion energy between the $1s$ and the $2s$ electron is only $5.71eV$. The sum of these energies are smaller than U and consequently a more accurate wavefunction would include partial occupation of this orbital to reduce the intra-atomic Coulomb repulsion. It can be shown that in this scenario the total system energy would be $-13.89eV$, much lower than the $-10.20eV$ for double $1s$ occupation. The exact energy for H^- is known to be $-14.36eV$ [39] a

result which could be approached by allowing the two electrons to partially occupy other atomic orbitals besides the $1s$ and $2s$ states. The essence of this behaviour can be captured without resorting to a complex multiple orbital per site Hamiltonian. The low energy behaviour may be mapped onto an effective single band tight-binding Hamiltonian provided that the single particle hopping amplitude be allowed to vary with the electronic occupation of the two sites involved. These arguments have led to to a $1D$ Hubbard-like model which on performing a particle-hole transformation can be written in terms of holes as [2]

$$\begin{aligned} H &= -t\sum_{i,i+1}(c^{\dagger}_{i,\sigma}c_{i+1,\sigma}+h.c.)+U\sum_{i}n_{i,\uparrow}n_{i,\downarrow}+V\sum_{i,i+1}n_{i}n_{i+1} \\ &\quad -\Delta t\sum_{i,i+1}(c^{\dagger}_{i,\sigma}c_{i+1,\sigma}+h.c.)(n_{i,-\sigma}+n_{i+1,-\sigma}), \end{aligned} \tag{2.15}$$

where the $c^{\dagger}_{i,\sigma}(c_{i,\sigma})$ are *hole* creation and destruction operators, U is the usual Hubbard on-site screened Coulomb repulsion and V is the intersite Coulomb interaction. The Δt term is an *off-diagonal* Coulomb matrix element

$$\Delta t = \langle i\ i|1/r|i\ i+1\rangle. \tag{2.16}$$

The Δt interaction term only becomes active when the site from which or to which the hole is hopping is already occupied by a hole. Thus there is an overall increase

[2] While the physics in either representation must be the same, it turns out (Chapter 3) that the *hole* formalism is more amenable to numerical lattice studies.

in kinetic energy for holes when other holes are present. The Δt term is sometimes referred to in the literature as the *bond-charge interaction* term. In this model it is assumed that

$$\Delta t = \alpha t, \tag{2.17}$$

with $\alpha > 0$. The supposition that the hopping interaction is proportional to the hopping is viable considering that both terms are derived by the same overlap matrix element of whichever electronic orbitals are involved. The magnitude and sign of Δt has been the subject of much debate [39, 40]. Nevertheless it is to be accepted as positive and non-zero although small compared to U throughout this thesis.

The single particle hopping amplitude t, is actually modified by the Hartree terms that arise from the Δt interaction in the above Hamiltonian. The hopping gets renormalized to the effective value

$$t(n) = t + n\Delta t, \tag{2.18}$$

where n is density of hole carriers present. This in turn implies that the non-interacting $1D$ bandwidth, $D = 4t$ is also now density dependent

$$D(n) = 4(t + n\Delta t). \tag{2.19}$$

Within tight-binding models, the hopping strength is inversely proportional to the effective mass m^*. Thus the above two equations show that as the number of holes in a band increases the hopping amplitude and bandwidth increase which signifies a decrease in the effective mass. That is to say, the effective mass for holes at the top of the band is larger than that for electrons at the bottom of the band. When written in terms of electron operators, the effective hopping for electrons in the Δt model is given by

$$t^e(n) = t^e - n\Delta t, \tag{2.20}$$

which in essence re-iterates the above statements concerning electron-hole asymmetry. Clearly the electron representation for $n > 1$ is equivalent to the hole formalism for $n < 1$. In this thesis the hole Hamiltonian is utilized but more will be said about the *electron* Δt model in Chapter 3.

The hole Hamiltonian admits a reduced interaction between Cooper pairs of the following form

$$V_{k,k'} = U + V\sum_{\vec{\delta}} e^{i(\vec{k}-\vec{k}')\cdot\vec{\delta}} - 2\Delta t\sum_{\vec{\delta}}(e^{i\vec{k}\cdot\vec{\delta}} + e^{i\vec{k}'\cdot\vec{\delta}}) \tag{2.21}$$

where $\vec{\delta}$ sums over coordinates. At the bottom of the hole band ($\vec{k} = \vec{k}' = 0$) the pairing interaction becomes

$$V_{0,0} = U + zV - 4z\Delta t \tag{2.22}$$

while at the top of the hole band ($\vec{k} = \vec{k'} = \pi$),

$$V_{\pi,\pi} = U + zV + 4z\Delta t, \tag{2.23}$$

with z the number of nearest neighbours equal to two in 1D. Clearly the interaction is less repulsive in the dilute hole limit. These equations emphasize that occupation near the top or bottom of the band has significant consequences with regards to the net effect of the Coulomb repulsion. Throughout this thesis V will be taken to be zero as its inclusion is not expected to overly influence the robustness of observed properties [3].

2.5.1 BCS Theory for the Δ t Model

The Δt model has been studied rigourously within BCS theory by Marsiglio and Hirsch [41] and Hirsch [42]. This model is found to exhibit superconductivity in the *dilute* hole regime without explicitly introducing an attractive Coulomb interaction, as is done, for example, in the attractive Hubbard Model. Pairing originates in a gain of kinetic energy rather than potential energy as is the case for conventional BCS

[3]The effects of including V on the properties of this model are reported in reference [41].

superconductors. That is, when particles pair their mobility increases and the total energy is lowered. [4]

The derivation of the Δt BCS equations proceeds analogously to the procedure outlined in Chapter 1. To begin the reduced Hamiltonian in k-space is defined as

$$H = \sum_{k,\sigma}(\epsilon_k^o - \mu)c_{k,\sigma}^\dagger c_{k,\sigma} + \frac{1}{N}\sum_{k,k',q} V_{k,k',q}c_{k,\uparrow}^\dagger c_{-k+q,\downarrow}^\dagger c_{-k'+q,\downarrow}c_{k,\uparrow}, \tag{2.24}$$

where the band dispersion is

$$\epsilon_k^o = -2t\cos k, \tag{2.25}$$

and

$$V_{k,k',q} = U + \frac{\Delta t}{t}(\epsilon_k^o + \epsilon_{-k+q}^o + \epsilon_{k'}^o + \epsilon_{-k'+q}^o). \tag{2.26}$$

The self-consistent superconducting gap and number density equations at zero temperature are obtained as

$$\Delta_k = \frac{-1}{N}\sum_{k'}[U + \frac{2\Delta t}{t}(\epsilon_k^o + \epsilon_{k'}^o)]\frac{\Delta_{k'}}{2E_{k'}}, \tag{2.27}$$

[4]Interestingly, another albeit different theory that utilizes kinetic energy arguments to account for high-T_c superconductivity is Anderson's *inter-plane tunneling* theory [43].

$$n = 1 - \frac{1}{N}\sum_k \frac{\epsilon_k - \mu}{E_k}, \tag{2.28}$$

where the single particle dispersion is renormalized to

$$\epsilon_k = \epsilon_k^o(1 + \frac{n\Delta t}{t}), \tag{2.29}$$

and the quasi-particle energy is

$$E_k = \sqrt{(\epsilon_k - \mu)^2 + \Delta_k^2}. \tag{2.30}$$

Clearly Equation 2.27 suggests the following form for the gap

$$\Delta_k = \Delta_m(c + \cos k), \tag{2.31}$$

where

$$\Delta_m = \frac{4\Delta t}{N}\sum_{k'} \frac{\Delta_{k'}}{2E_{k'}}, \tag{2.32}$$

and

$$c = \frac{-1}{N}\sum_{k'}(U + \frac{2\Delta t}{t}\epsilon^o_{k'})(c - \frac{\epsilon^o_{k'}}{2t})/2E_{k'}. \tag{2.33}$$

At finite temperature in the weak coupling limit an analytic expression for the critical temperature T_c and gap function are found to be [41]

$$T_c = \frac{e^\gamma}{\pi} D_n \sqrt{n(2-n)} e^{-a/b}, \tag{2.34}$$

$$\Delta_o = D_n \sqrt{n(2-n)} e^{-a/b}, \tag{2.35}$$

where D_n is the renormalized bandwidth and $\frac{-a}{b}$ is a density-dependent density of states factor. Roughly speaking the exponential may be re-written as

$$e^{-1/N(\epsilon)V}, \tag{2.36}$$

which at low density approaches one due to the divergence of the 1D density of states (Section 2.4) and thus

$$\Delta_o \sim 4t_n \sqrt{n(2-n)}. \tag{2.37}$$

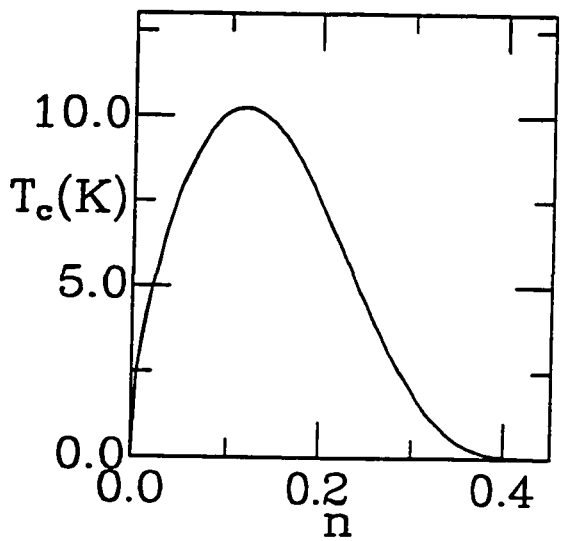

Figure 2.5: T_c vs. Carrier Density

Clearly at low density both the gap function and T_c within BCS theory rises as the hole carrier density increases. Figure 2.5.1 shows the typical behaviour of T_c with hole concentration as given by Equation 2.34 for a 1D density of states.

The Schrödinger equation for two holes yields an analytic condition on the parameters that give rise to the pairing of the holes [42]. Furthermore, it was demonstrated [44] that this condition coincides with the case for non-zero T_c obtained from BCS theory in the zero density hole limit in $1D$ and $2D$. The restriction for hole pairing is

$$\frac{\Delta t}{t} > \sqrt{1 + \frac{U}{2zt}} - 1. \tag{2.38}$$

The density range n_c beyond which superconductivity vanishes within weak coupling BCS theory is determined by the requirement

$$0 = \frac{2\Delta t}{t}(1 - n_c) - \frac{U}{4t} + (\frac{\Delta t}{t})^2(1 - n_c + \frac{n_c^2}{2}). \tag{2.39}$$

2.5.2 The Δt Model and High-T_c Oxides

It has been argued [37, 38, 41, 42] that the characteristic doping asymmetry between electrons and holes portrayed by the Δt model underlies the origins of superconductivity in the high-T_c oxides. That is, holes conducting through O^{2-} anions in the copper-oxide planes will tend to pair when hopping in the presence of other holes. This scenario is consistent with an electronic structure based on a 3-band Hubbard model. The physics of this model is hypothesized to explain *only* the superconducting behaviour of the high-T_c oxides as holes are doped into a full band. A *complete* model describing the magnetic aspects of the HTSCs would necessarily have to take the copper $d_{x^2-y^2}$ orbitals into account. Nevertheless, the Δt model posesses several features which make it a viable candidate for discussing high temperature superconductivity. The behaviour of T_c with hole doping in the high-T_c oxides is captured by the Δt model in BCS theory as shown by Figure 2.5.1. This model could be applica-

ble to non-magnetic oxides such as $Ba_{1-x}K_xBiO_4$. It has also been pointed out [45] that superconductivity in solids is correlated to a positive value of the Hall coefficient thereby indicating that holes are the carriers.

As previously mentioned, BCS superconductivity in the Δt model is driven by kinetic energy or hopping processes. Specifically, the gap equation depends explicitly on the band energy (Equation 2.31) which is manifest of the hopping process. Thus the superconducting state is *intrinsically* isotropic because as the band structure or Fermi surface varies, the gap varies along with it in the same manner. While the hole-doped superconductors appear to have an anisotropic gap, the same cannot be said for electron-doped superconductors.

In this thesis the $1D$ properties of the Δt model will be characterized while greater detail for its motivation can be found in the references given at the beginning of this section.

Chapter 3

Exact Diagonalization Studies

3.1 Construction and Diagonalization of Hamiltonian Matrices

This thesis examines the numerical modelling of strongly interacting electrons on finite lattices. A major component of such studies is the construction of the Hamiltonian matrix for the system in question which is then subsequently diagonalized to yield the system eigenvalues and eigenvectors. This process is commonly referred to as *Exact Diagonalization* and is *only* limited by the size of the Hilbert space or order of the matrix to be diagonalized.

The process by which the Hamiltonian matrix is constructed will be illustrated using the $1D$ Hubbard model. Nevertheless the procedure is the same for the Δt model. To start, consider the possible electronic configurations or basis states for a single lattice point. Keeping in mind the Pauli Exclusion Principle, there can be arrangements with zero, one, and two electrons per site. Specifically the states are designated as $|0\rangle$, $|\uparrow\rangle$, $|\downarrow\rangle$, $|\uparrow\downarrow\rangle$, representing, the vacuum state, a single spin-up particle, a single

spin-down particle, and a doubly occupied spin-up and spin-down state respectively. Note the order of spins on the doubly occupied site. Throughout the thesis this order, *spin-up first*, will be used although the opposite order could equally well have been chosen. The important point is that the order is consistently maintained since electrons are fermions and they anti-commute with one another [1]. Therefore, in general a 1D Hubbard chain of L sites has 4^L possible basis states. The Hamiltonian matrix is square in dimension and its order is given by the number of basis states. The basis states or Hilbert space for an L site chain can be generated by taking the tensor product of each site's basis states with all the others i.e.,

$$|1\rangle \otimes |2\rangle \otimes |3\rangle \otimes \ldots |L\rangle$$

where $|i\rangle$, $i = 1, 2, 3, \ldots, L$, represents all the basis states for site i. Each matrix element is then computed by operating the Hamiltonian on each of the individual basis states α by

$$H_{\alpha,\beta} = \langle\beta|H|\alpha\rangle.$$

For a chain of 12 sites the number of basis states is 4^{12} or 16,777,216. While a chain this length may be considered small, a matrix of this dimension is far and away too enormous to be diagonalized. However all is not lost as the Hamiltonian posesses certain symmetries which can reduce the size of the matrix that needs to

[1]This concept of order is particularly important in the Density Matrix Renormalization Group calculations to be discussed later.

be diagonalized. In particular there are no terms in the Hubbard Hamiltonian which flip spins or create or destroy extraneous particles. That is to say, the Hamiltonian conserves spin and particle number [2] . Furthermore, translational invariance in real-space directly implies the conservation of momentum in k-space. Each basis state may then be identified with a unique set of quantum numbers for total momentum (K_{tot}), spin (S_z), and particle number (N). The upshot of these symmetries is that the Hamiltonian matrix can be made block diagonal in these quantum number sectors and rather than diagonalizing the matrix for the entire Hilbert space, each smaller block can be diagonalized individually. For example, in the two site problem there are 16 basis states in total but the largest block in the Hamiltonian matrix is of dimension 4x4 for the *sector* with $N = 2, S_z = 0$, and $K_{tot} = 0$. In addition this happens to be the sector where the ground state for the entire system lies although in general each sector must examined for this possibility [3]. It is worth emphasizing the fact that the above example is a trivial system and often much larger systems must be studied which contain blocks that cannot be diagonalized in their entirety using conventional routines such as Householder's method [46]. Fortunately, in many cases the ground state energy E_o, and the ground state wavevector Ψ_o, are adequate enough to characterize the low temperature properties of a system thereby making a complete or dense diagonalization unnecessary. In this case a technique known

[2]In group symmetry terms, a Hamiltonian that conserves spin posesses SU(2) symmetry while the conservation of charge or particle number is designated by the symmetry U(1).

[3]In some cases additional knowledge may be used to *guess* which sector contains the ground state. For example, in the 1D Hubbard model the ground state must be a singlet.

as the *Lanczos* method [47, 48] may be implemented to diagonalize the matrix in question. The advantage of this process is that a few eigenenergies and eigenvectors of extremely large sparse matrices may be obtained. Typically a *sparsity* [4] of less than 5% is desirable.

Many standard Lanczos algorithms are available and in most instances it may be sufficient to treat such routines as 'black boxes'. However, the concepts are straightforward enough that one could write their own routine. Furthermore, exact diagonalization studies employing a Lanczos routine can be utilized to obtain dynamical response functions such as spectral densities. For further discussion see [48].

The algorithm is an iterative method whereby a *special* basis can be constructed using the basis of the original Hamiltonian. In this representation the original matrix can be partially tridiagonalized and the extremal eigenvalues of the initial matrix can be extracted. The accuracy of Lanczos results will be discussed in the sections that follow. Exact diagonalization routines are an integral part of the recently developed real space numerical studies called the Density Matrix Renormalization Group. This technique is the focus of Chapter 4.

3.2 Pair Binding

In this thesis the binding energy of two particles within Hubbard-like models will be extensively studied. While pair binding does not guarantee the existence of a

[4] The sparseness of a matrix is represented by the ratio of the number of non-zero elements to the maximum number of possible elements (this is simply given as the dimension of the matrix squared).

superconducting condensate, it is an essential ingredient for Cooper pair formation and the onset of superconductivity. Moreover, a clear distinction must be made between pair formation and superconductivity, versus phase separation. In general the pair binding energy is defined as

$$E^{bind}(N) = 2E_o(N) - [E_o(N+1) + E_o(N-1)] \tag{3.1}$$

where $E_o(N)$ represents the ground state energy of a many body system with N particles added to it, N being an odd number. For finite lattice studies even and odd particle densities are easily kept track of while in the thermodynamic limit (Bethe Ansatz) this differentiation is lost. Consequently finite size effects must be checked. The binding energy can be used to define the single particle or *charge-transfer gap* as

$$\Delta_c(N) = E^{bind}/2. \tag{3.2}$$

This name is misleading as it implies the existence of an order parameter while the above equation is only indicative of whether attractive forces are at work. $E_o(N)$ is obtained from the diagonalization of the appropriate Hamiltonian matrix and is negative in value. Simply stated, E^{bind}, represents the difference in energy between two non-interacting particles and that of two interacting particles in a many body system. As defined above when E^{bind} is positive a pair of interacting particles forms a

bound state. Generally the pair binding energy is a small difference of large numbers and hence individual energies must be computed with high precision.

It should be noted that a negative binding energy is not physical and it typifies a finite size effect. A negative value of E^{bind} implies that the interaction between two particles is repulsive. In the thermodynamic limit then, two particles will tend to stay as far apart as possible and are essentially non-interacting. Thus E^{bind} has a minimum of zero as there would be no distinction between interacting and free particles.

A positive value for E^{bind} could also signify particle clustering or a system's tendency to phase separate. To test for phase separtion the binding energy of three particles with respect to splitting into a pair and a single particle can be calculated as [49]

$$E^{bind,3} = [E_o(3) + E_o(0)] - [E_o(2) + E_o(1)]. \tag{3.3}$$

Similarly the binding of four particles with respect to double pair formation would be

$$E^{bind,4} = [E_o(4) + E_o(0)] - 2E_o(2). \tag{3.4}$$

$E^{bind,3}$ and $E^{bind,4}$ would both be positive if phase separation did not occur.

3.3 Spin Gap

An alternate measure of pairing is provided by the *spin* gap. A gap in the spin excitation spectrum for a fixed number of particles is defined by

$$\Delta_s = E(S_{tot} = 1) - E(S_{tot} = 0), \tag{3.5}$$

where $E(S_{tot})$ is the ground state energy in the particle subspace with fixed spin. The spin gap denotes the lower critical magnetic field required to flip a spin and break up a singlet pair. This field is zero in the absence of a spin excitation gap. Unlike the charge gap, calculation of the spin gap is amenable to Bethe Ansatz techniques only in the thermodynamic limit.

3.4 Discussion of Exact Diagonalization Studies

3.4.1 The Hubbard Model

Exact diagonalization studies have been performed for the 1D Hubbard and Δt models on chains up to 12 sites in length. In order to ensure that the numerical routines were functioning properly the 1D Hubbard model was studied within exact diagonalization and benchmarked against the true results as obtained from the Bethe Ansatz solution. One may be led to question the significance of performing exact diagonalization studies for this model when the true result is provided by the Bethe Ansatz solution. The reason for this is to provide a reliable technique to study any model

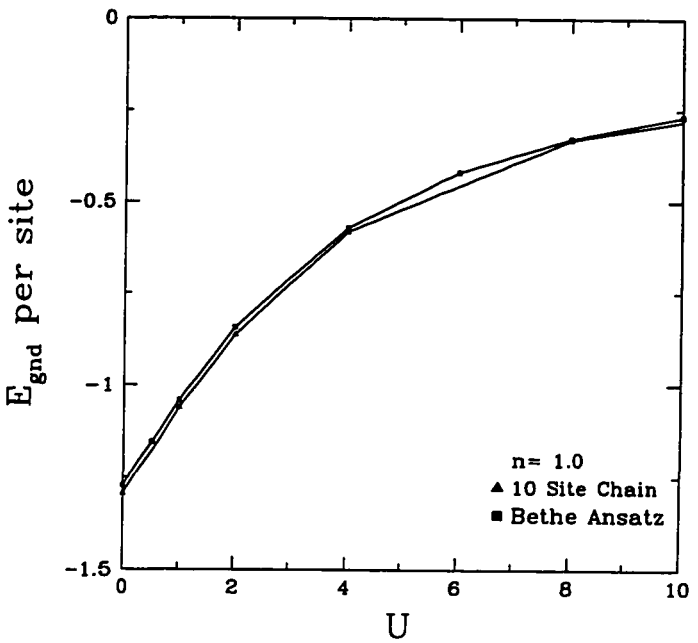

Figure 3.1: Comparison of the Ground State Energy vs. Hubbard Coupling for a 10 Site Chain and the Bulk Limit.

where the true solution is not known. To compare results the analytic expressions from the Bethe Ansatz listed in the previous chapter were used. In Figure 3.1 the ground state energy for a 10 site Hubbard chain is plotted against the repulsive interaction strength U at half filling ($n = 1$). For each value of U examined over the entire range of coupling strengths there is good agreement between the exact diagonalization and Bethe Ansatz results. In Figure 3.2 the ground state energy at $U = 8.0t$ is plotted against number density for chains of length 6, 8, 10, and 12 sites. This plot illustrates several features. First this graph serves as a check on finite size effects in the system. As the lattice size increases from 6 to 12 sites the overall agreement

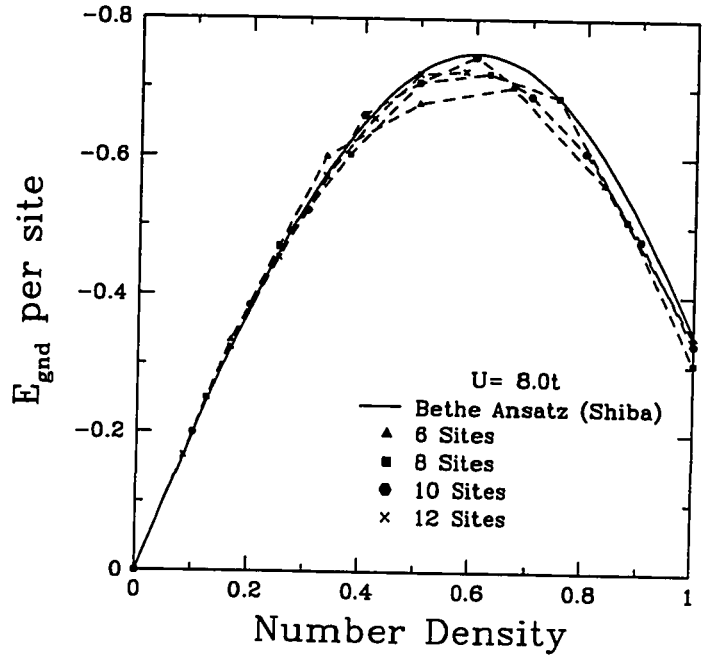

Figure 3.2: Variation of Energy with Lattice Size.

with the Bethe Ansatz result improves however it appears from examining the 8, 10, and 12 site chains that the energies are converging properly to the energies in the thermodynamic limit. For low densities ($n < 0.3$) there is excellent agreement for all the chains. It is safe to conclude that the ground state energies provided by exact diagonalization for the 1D repulsive Hubbard model are accurate.

In Figure 3.4.1 the exact diagonalization energy versus density for a 10 site chain is plotted as the interaction strength crosses over from the attractive ($U < 0$) to repulsive ($U > 0$) regime. In the cases of $U > 0$ the energy curves are relatively smooth functions of density while as U becomes increasingly negative the curves become more *ragged.* At first glance one might be led to the conclusion that the data

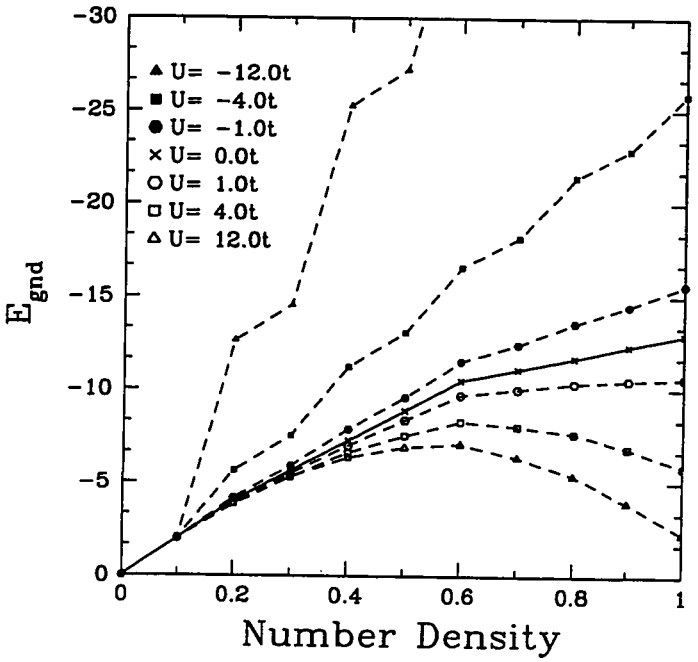

Figure 3.3: Energy vs. Density for Various Coupling Strengths for a 10 Site Chain.

in the attractive regime has a larger uncertainty which increases with decreasing U. However, the lack of *smoothness* in the $U < 0$ curves is simply attributed to the fact that the stronger the attraction the greater the distinction between even and odd numbers of particles in the system. In the attractive case particles prefer to be as *close* to one another as possible while the opposite is true for $U > 0$. That is there is an increase in the magnitude of the ground state energy on the order of $|U|$ when proceeding from an odd to an even number of particles. There is no *a priori* reason for taking the potential U to be negative without explaining how the repulsive Coulomb potential between two electrons is overcome. Consequently the attractive Hubbard model lacks credibility as a physical model compared to the more realistic

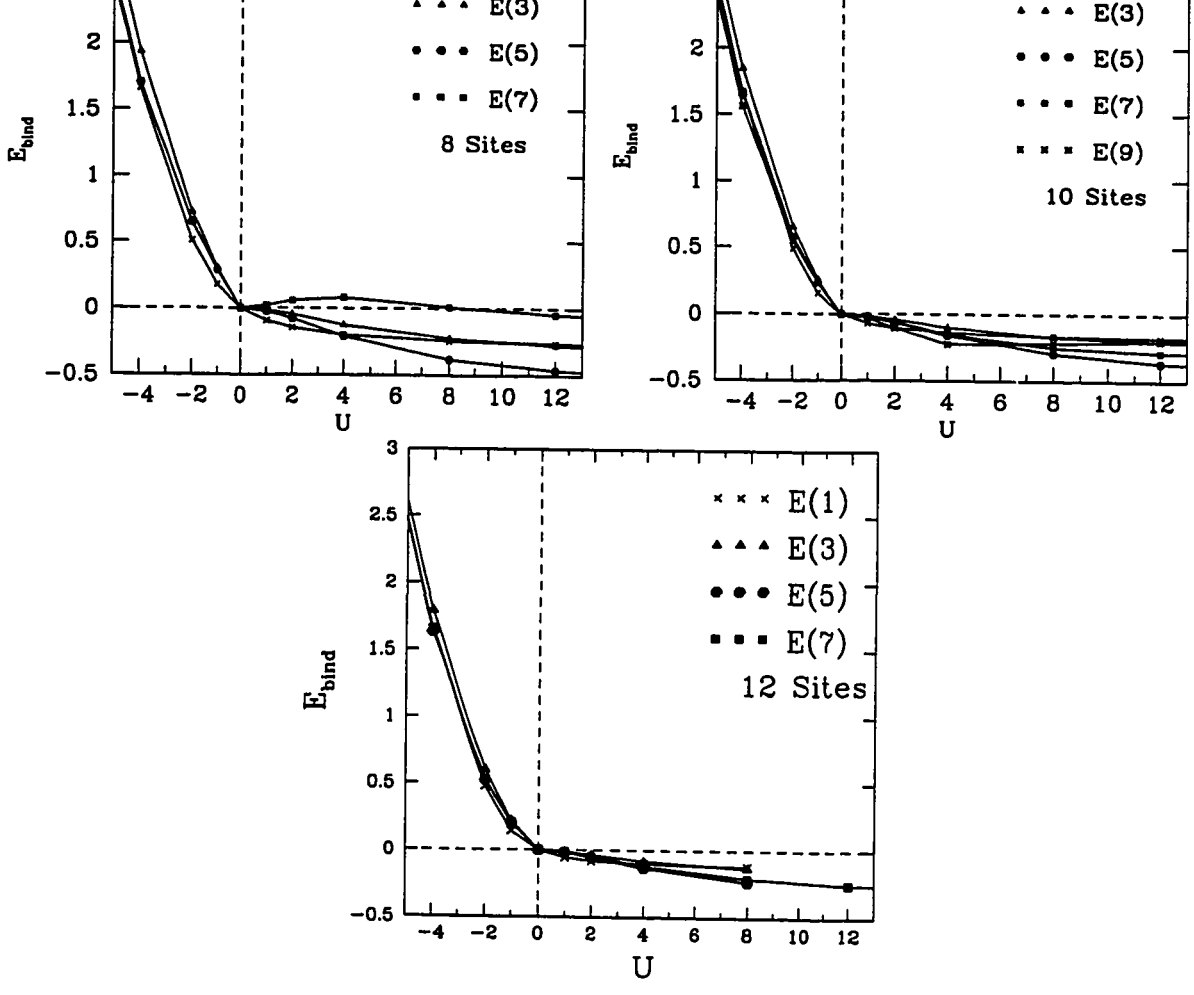

Figure 3.4: Binding Energy vs. U for an 8, 10, and 12 Site Chains

repulsive model.

The ground state energies are used to calculate the pair binding energies via Equation 3.1. As mentioned in the introduction there is no conclusive evidence for the existence of superconductivity in the repulsive Hubbard model. Various techniques have been used to search for superconducting signatures all varying in degrees of complexity. In order to assess the exact diagonalization procedure, studies were used to calculate binding energies in the $1D$ Hubbard chain. One could use the Bethe Ansatz

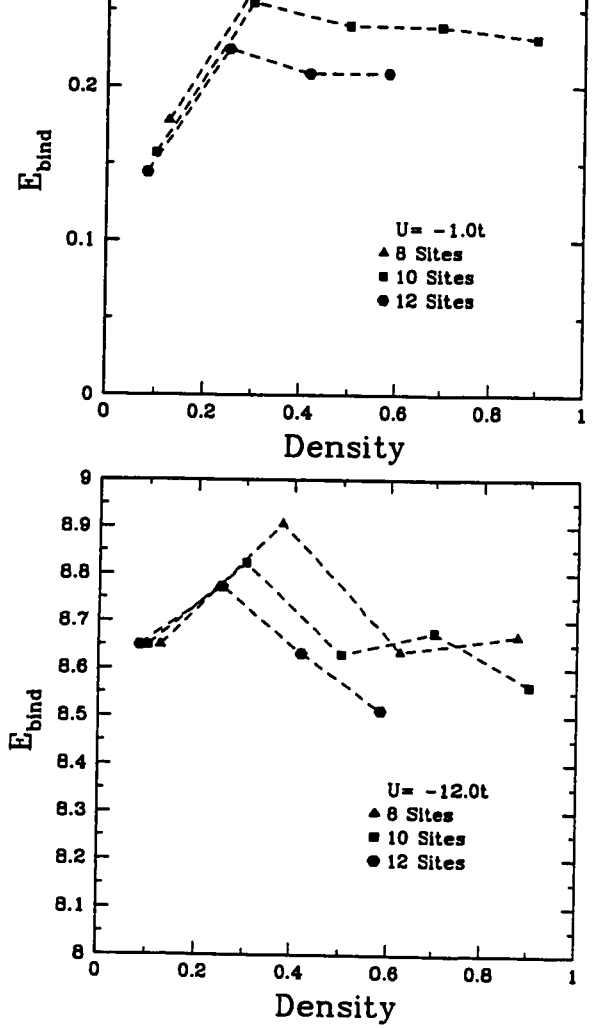

Figure 3.5: Pairing in the Attractive Hubbard Model for both Weak and Strong Coupling

to do this but as previously mentioned in the thermodynamic or bulk limit particle number distinction is lost so that Equation 3.1 is not applicable. In Figure 3.4 the binding energy is plotted against interaction strength for 8, 10 and 12 site chains with periodic boundary conditions. Recall that for $E^{bind} > 0$ there is pairing. In all three chain sizes for $U < 0$ there is pairing while for $U > 0$ the results are less clear. For the 8 site chain there is a small amount of binding in the range $0 < U < 9.0t$ for a pair of holes near half filling (curve E(7) on the plot). For all other densities available

there is no binding. As the chain length is increased to 10 sites there is no binding at any density for positive U. For 12 sites there is no binding for electron number densities up to 7/12 or 0.583. Computer resources prevented the investigation of pairing near half filling for the 12 site chain. While not shown, 4 and 6 site chains were also examined with there being a small degree of binding for a pair of holes in the 4 site case and no binding whatsoever in the 6 site case. Thus as there is binding in the 4 an 8 site chains for a pair of holes it could be the case that there is also binding in the 12 site case. However since there is no binding in the 6 and 10 site cases it is likely that the binding is an artifact of finite size effects. A study addressing the binding of holes in the 1D Hubbard chain was carried out by Fye et. al [50]. They used Bethe Ansatz equations to calculate binding energies just off half filling. To check that their procedure was functioning properly they also made extensive comparisons with exact diagonalizations results for 2, 4, 6, 8 and 10 sites. What this work showed was the existence of binding in chains with periodic boundary conditions of length $N = 4i$ and binding in chains of length $N = 4i + 2$ with anti-periodic boundary conditions. Specifically for 4, 8, and 16 sites the binding increased in range and magnitude as the lattice size increased. The fact that the range over U in which binding occurs actually increases with increasing lattice size is non-intuitive as the larger the lattice is, the more *room* there is for electrons to spread out and avoid one another. However, when a 64 site chain was examined there was binding *but* it decreased in going from 16 to 64 sites. These results suggest that the pairing is a finite size effect and eventually

vanishes in the thermodynamic limit as expected. Moreover this study serves notice that extreme caution must be used in studying finite size systems in order to separate artefact from reality.

As already shown in Figure 3.4 the attractive Hubbard model displays pairing. In Figure 3.5 the binding energy is plotted against electron density for 8, 10 and 12 site chains as the coupling strength changes from weak ($U = -1.0t$) to strong ($U = -12.0t$) coupling. In weak coupling the binding energy at first increases with density then as the density continues to increase the binding energy decreases monotonically. As the lattice size increases there is a downward shift in the magnitude of the binding energy at intermediate to high densities. In the low density regime there is good agreement between binding energies for all three lattice sizes. In the strong coupling regime finite size effects are less prominent and there is less variation of the pairing energy with density.

3.4.2 The Δt Model

Now the Δt model will be addressed. Recall that in extending the Hubbard model to form the Δt model, it has been shown (within the BCS approximation) that superconductivity exists for a certain range of model parameters. In Figure 3.6 the effect of lattice size on the ground state energy as a function of density is plotted for $U = 0t$ and $\Delta t = 1.0t$. It should be pointed out that the ground state energy path of convergence depends on whether the lattice contains an even number of particles or odd. For example, at a density $n = 0.5$ the ground state energy per site for a 6

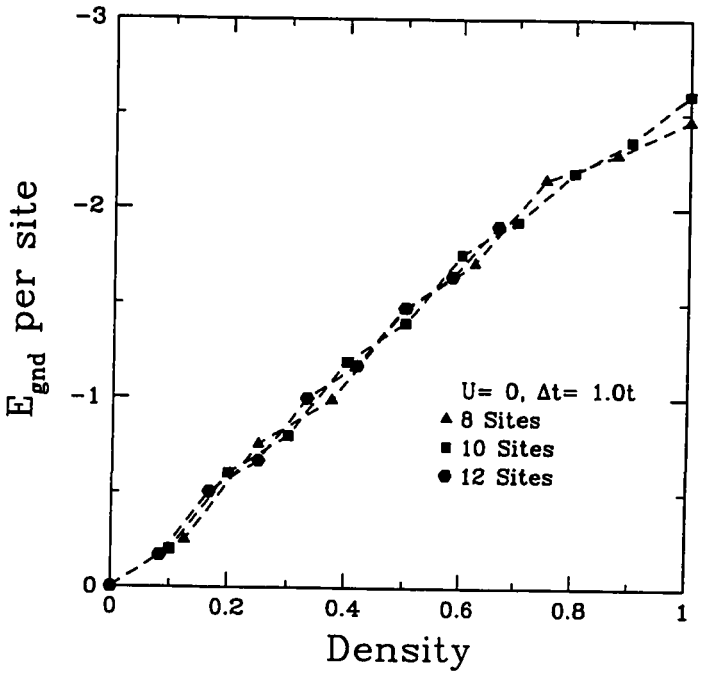

Figure 3.6: Ground State Energy vs. Density for Various Coupling Strengths in the Δt Model

site lattice (not shown on the plot) is approximately $-1.2896t$, while for the 8, 10, and 12 site cases the energies are $-1.4697t$, $-1.3954t$, and $-1.4757t$, respectively. At this filling, there are an odd number of particles on the 6 and 10 site chains (3 and 5 particles, respectively) and an even particle count on the 8 and 12 site chains (4 and 6 particles, respectively). This behaviour can be attributed to the difference in energy between the singlet ground state of the evenly occupied chain and the doublet ground state of a chain with an odd particle number occupation. In the thermodynamic limit both energy sequences must eventually converge to the same value as the discernment between even and odd occupations is inconsequential.

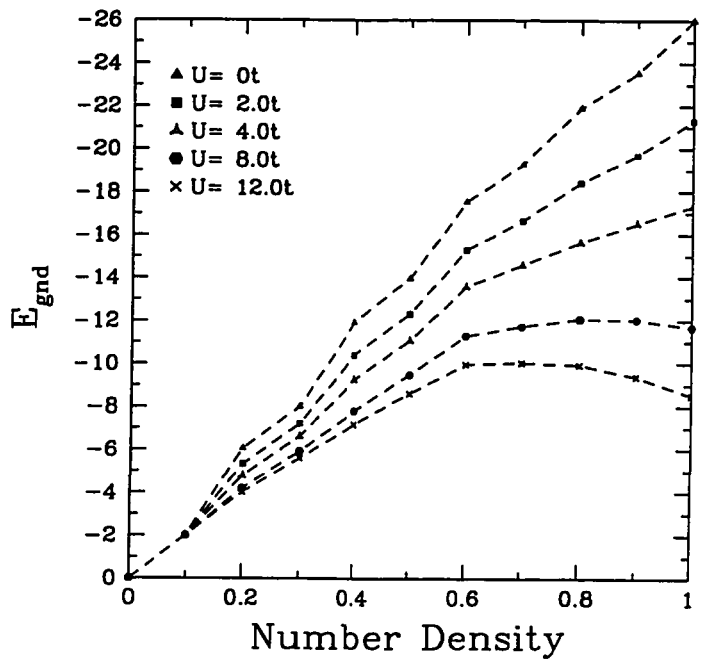

Figure 3.7: Ground State Energy vs. Density for Various Coupling Strengths in the Δt Model

Nevertheless, the deviation between the curves for all three lattice sizes at all densities is relatively small indicating that convergence is adequate.

In Figure 3.7 the ground state energy for the Δt model is plotted against hole number density for $\Delta t = 1.0t$ and various positive values of U. As U is decreased in magnitude the corresponding curves follow behaviour similar to that shown in Figure 3.4.1 as there is a crossover from the repulsive to the attractive regime. However unlike Figure 3.4.1 U is always repulsive in this case. Moreover this plot suggests that as U is decreased the effect of the Δt term becomes more dominant. This is in direct agreement with the BCS prediction of the constraints on Δt as a function of U

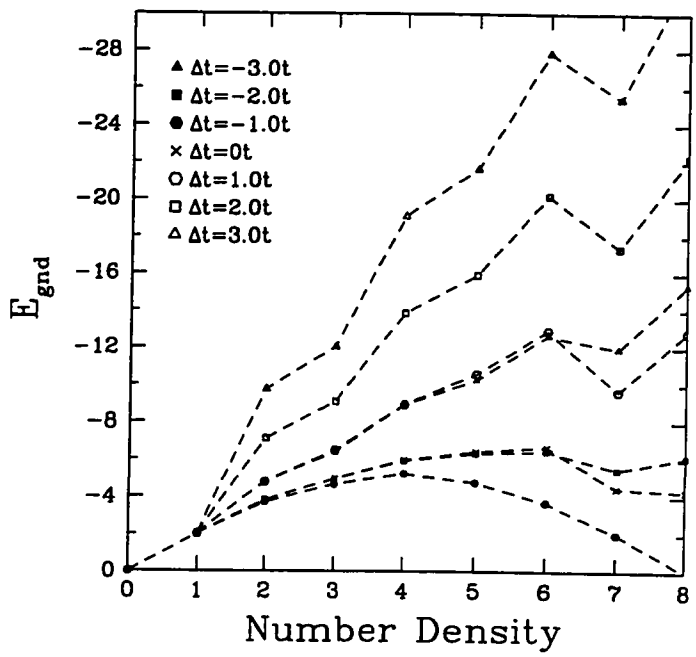

Figure 3.8: Ground State Energy vs. Density for Various Coupling Values of Δt

(Equation 2.38). Also of note is that those curves which do display *choppiness* become smoother as the density increases thereby signifying less of a distinction between even and odd numbers of particles. The increased effect of Δt on the energy is displayed in Figure 3.8 as U is held fixed. As Δt increase the curves display a higher degree of structure reminiscent of the behaviour in Figure 3.4.1 for $U < 0$.

The binding energy for various allowed hole densities versus U is plotted in Figure 3.9 for 8, 10, and 12 site chains. In each case the parameter $\Delta t = 1.0t$. Keep in mind that there are constraints on the allowed densities so that the actual data is represented by the symbols while the lines are just a guide to the eye. Also note that the curve depicted by $E(1)$ represents the low density or dilute limit of hole carriers

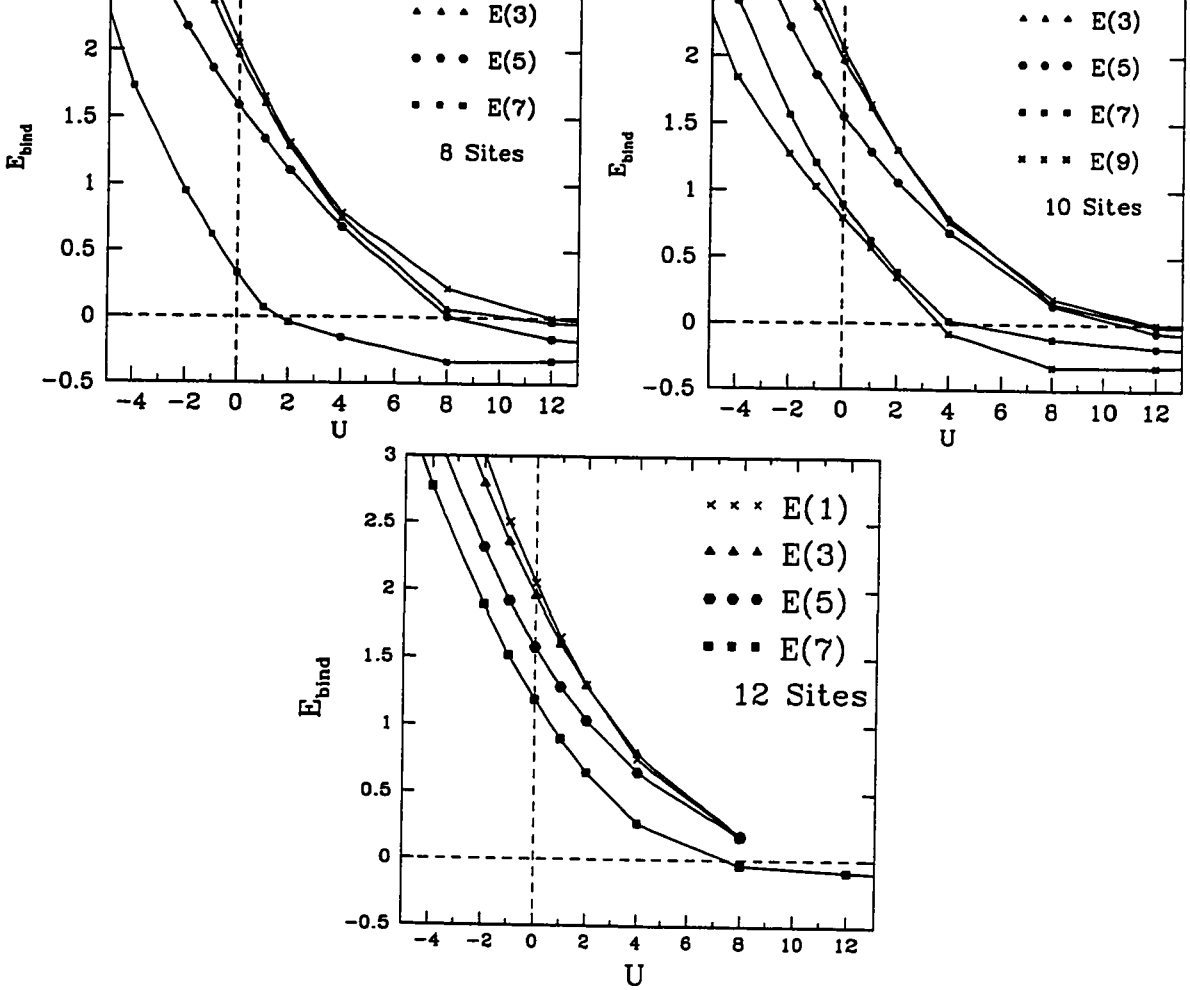

Figure 3.9: Binding Energy vs. U for an 8, 10, and 12 Site Chains in the Δt Model

and that the density for $E(1)$ in the 8 site case is not at the same density for $E(1)$ in the 10 site case. In the former the density is $1/8 = 0.125$ while in the latter it is $1/10 = 0.100$. These plots show that there is pair binding for a wide range of potential. Furthermore the finite size effects are small as the critical potential U_c at which binding disappears changes little as the lattice size changes. A very important feature of these curves is that the binding is density dependent. For constant U as the number of holes increases the binding decreases ($E(1) > E(3) > E(5) > \ldots$) in direct

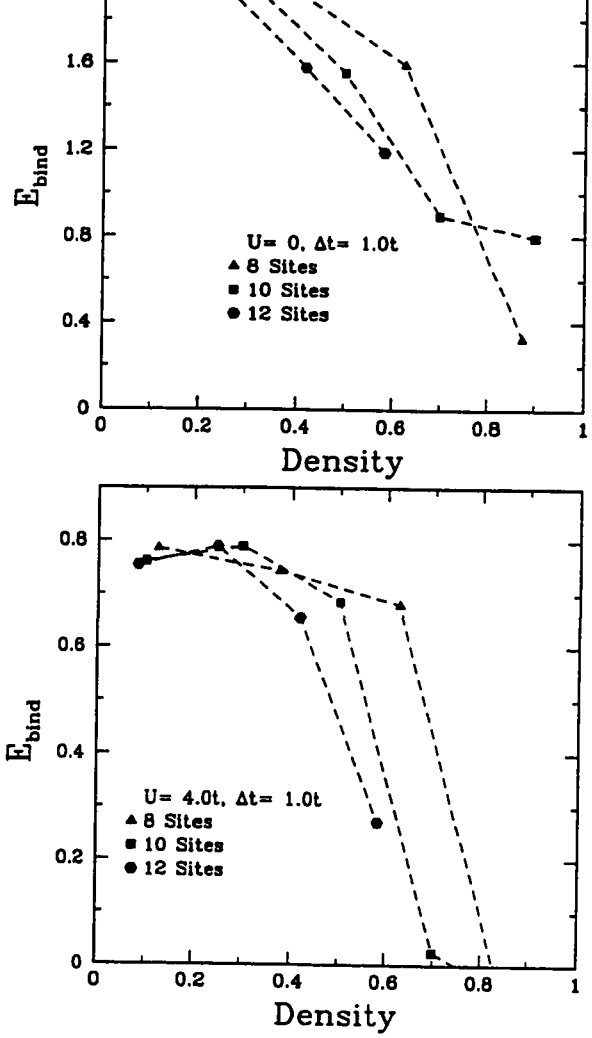

Figure 3.10: Binding Energy vs. Density for an 8, 10, and 12 Site Chains in the Δt Model

agreement with the BCS model predictions. The density at which binding disappears is in similar agreement with the predictions of BCS theory in Chapter 2 as is the constraint on parameter values necessary for binding. In particular, for $\Delta t = 1.0t$ and $U = 4.0t$ BCS theory predicts that pairing will occur only up to a critical carrier density of $n \approx 0.764$. Also for $\Delta t = 1.0t$ pairing will only occur if $U < 12t$. Inspection of the binding energy curves in Figure 3.9 shows that both theses conditions are met. In Figures 3.10 the pair binding energy is plotted against hole density for various

paramaters and lattice sizes. Here the qualitative features of the binding energy curves show variation with parameter values and are not overly influenced by finite size effects. For $U = 0$ and $\Delta t = 1.0t$ the binding energy decreases monotonically with increasing density. These results are contrary to BCS gap behaviour of this model as predicted by Hirsch and Marsiglio in Chapter 2. Also it is known [51] that BCS theory is exact in the weak and strong coupling limits. This discrepancy suggests that the agreement is only exact in the zero density limit. However, for decreased coupling strength the density dependence is less clear. For $U = 4.0t$ and $\Delta t = 1.0t$ in the 8 site chain the binding energy decreases with increasing density while for the 10 and 12 site chains the binding at increases at first with density then decreases as the density continues to increase. Similar behaviour is observed for the parameters $U = 8.0t$ and $\Delta t = 1.0t$. Note that $U = 0$ and $\Delta t = 1.0t$ is at stronger coupling than $U = 4.0t$ and $\Delta t = 1.0t$ as is reflected by the difference in energy scales. In weak coupling it appears that finite size effects for the smallest lattice size are still too significant and that the true behaviour of the binding energy follows that predicted by BCS theory. The fact that the binding energy curves in strong coupling do not conform qualitatively to BCS predictions appears puzzling and prompts further study. In addition no evidence of phase separation was found.

3.5 Other Studies of the Δt Model

Hirsch and Lin [52] have also studied pairing in the Δt model within exact diagonalization studies and made comparisons to BCS predictions. In particular they

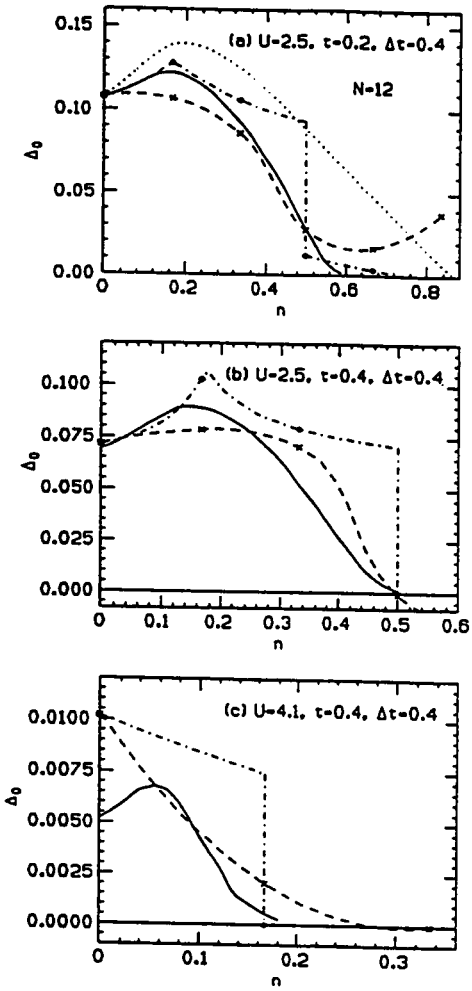

Figure 3.11: Gap versus Density in the Δt Model

attempted to classify the density range over which BCS theory is accurate. As previously mentioned BCS theory is in a sense a mean field approximation which accurately describes pair binding but does account for interactions between pairs except for the Pauli Exclusion Principle. They presented energy gap versus density results for finite size and bulk systems and came to the overall same conclusion in both cases.

Their exact results (Figure 3.11) were presented for a 12 site chain while BCS predictions were given for the infinite and 12 site systems. The infinite BCS results are

given by the solid curve while the finite BCS results are given by the dash-dot curve. Exact diagonalization data is represented by the dashed curve. Data for three sets of parameters was used, $U = 2.5$, $t = 0.2$, $\Delta t = 2.0$, $U = 2.5$, $t = 0.4$, $\Delta t = 1.0$, and $U = 4.1$, $t = 0.4$, $\Delta t = 1.0$ which correspond to strong, intermediate, and weak coupling regimes respectively. In all three coupling ranges the infinite size BCS gap versus density had the behaviour as presented in Chapter 2. That is, as a function of density the magnitude of the gap at first rises with hole density, reaches a maximum, and then decreases as the density increases until it vanishes at the maximum density as given by Equation 2.39. For the strong and intermediate coupling cases the finite size BCS plots display the same qualitative behaviour as in the infinite size scenario. However, for the weak coupling strength the gap does *not* increase with density but decreases monotonically with denisty. For the 12 site chain the pair binding energy decreases as a function of increasing carrier concentration for the strong and weak coupling regimes but increases slightly in the intermediate region. The authors claim that this overall decrease in the exact case is due to the limited discrete values of density that can be probed. While the effect of finite size on the exact solution is not formally presented, the authors state that "... from results for a large set of lattices and parameter ranges we conclude that also in the exact solution the pair binding always first increase as the density increases from zero for a sufficiently large lattice." The evidence presented does not conclusively support this conjecture and if anything may suggest otherwise.

In the limit of zero carrier density the exact and BCS results are in good agreement except for the weak coupling case. Although no mention is made, it turns out that the cause of this disparity is finite size effects (more will be said about this later). The range over which pair binding occurs is less for the BCS solution than it is for the exact case.

The study also showed there was no tendency towards phase separation or particle clustering.

3.6 Electron Δt Model

One could also study the *electron* version of the Δt Hamiltonian. Recall that this Hamiltonian is identical in form to the hole Hamiltonian except that the sign of Δt is negative in this case. The physics is similar in that there is pairing of holes in the dilute hole limit or the limit of a filled electron band. The handicap in using the electron Hamiltonian is that to probe the superconducting region one must keep track of a large number of electrons as opposed to a few number of particles in the hole case. Additionally, subtleties arise in the electron picture in that the renormalized single electron hopping amplitude

$$\tilde{t} = t - n_e \Delta t,$$

can change sign as Δt increases when the electron density n_e is on the order of one. That is, there is a range of parameters for which $\tilde{t}$ or the average hopping can go

to zero. Whether or not these values are physical remains to be determined. By adopting the hole picture this delicate *characteristic* can be avoided.

Nevertheless, some features of the Δt electron Hamiltonian have been investigated by Quassier et al. [53]. In particular they compare the electron Δt model to a modified version of the Δt model known as the *Bariev* model [54]. In the Bariev model Hamiltonian the effective hopping amplitude is given by

$$t^{Bariev} = t - \Delta t n_{i+(1+\sigma)/2,-\sigma}, \tag{3.6}$$

which is only one half of the original Δt interaction term. The significance of this model is that it can be solved precisely by Bethe Ansatz techniques. While this model does not contain the entire Δt *interaction* it does take correlated hopping into account and thus it is plausible that this model retains essential features of the original model. Exact diagonalization results for the two models are made on small chains for various values of Δt while U is always taken to be zero. For chain sizes up to 16 sites the ground state energy shows a good level of convergence. Furthermore, the energies of the Bariev model for exact diagonalization correspond well with the Bethe Ansatz solution. Thus finite size effects do not appear to be significant in this model. The gound state energy of the Δt model shows good correspondence with that of the Bariev model at small values of Δt while for $\Delta t = 1.0t$, there is a noticeable difference between the curves. In addition boundary conditions were varied in order to assess

the impact of restricted lattice size. Overall, the authors conclude that finite size effects are not serious and the ground state energy in the two models shows good agreement for small values of Δt.

The pair binding energy was also investigated on a 12 chain for both models at an electron density of 20/12. Binding is found to exist in both models however in the electron Δt model pairing vanishes beyond a critical value of $\Delta t \simeq 1.5t$. In the hole picture, for $U = 0$ there is binding for all values of $\Delta t > 0$. The pairing in the electron picture goes to zero because as mentioned earlier the effective hopping amplitude passes through zero as Δt is increased. The behaviour for this choice of parameters could be indicative of some ancillary action such as a metal-insulator or superconductor-insulator transition for which further study is required. The authors make no mention of this fact and should not have examined only the superconductivity in this case. This subtlety can be avoided by working within the hole description where only the the superconducting features can be probed. Investigations which examine the electron Δt model and superconducting transitions as well as possible non-superconducting transitions have been undertaken by Arrachea et al. [55] and by Airoldi and Parola [56].

3.7 Characterization of the BCS Approximation

Recently Marsiglio [57] has evaluated the BCS approximation for the attractive Hubbard model in one dimension. The essence of this study is to test the accuracy of the BCS theory by comparing its predictions to the true solution of 1D Hubbard

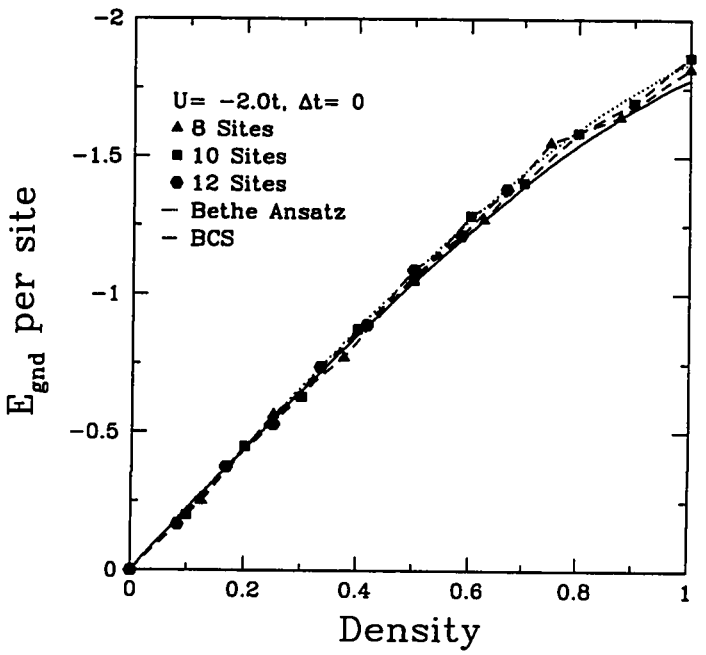

Figure 3.12: Ground State Energy for the Attractive Hubbard Model Case $U = -2.0t$

model which is provided by the Bethe Ansatz equations (Chapter 2). Specifically the ground state energy and energy gap to the first excited state were calculated using both the variational BCS wavefunction and the Bethe Ansatz technique. Furthermore the influence of finite size effects on the results in both cases was also investigated. Even though the exact solution to the 1D Hubbard model is known, the influence of finite size is beneficial to studies of similar models where only a numerical solution is possible.

In this study comparisons between the two procedures were provided as a function of the electron density and coupling interaction strength U. Note that the form of the attractive Hubbard Hamiltonian is identical to that of the repulsive case except for

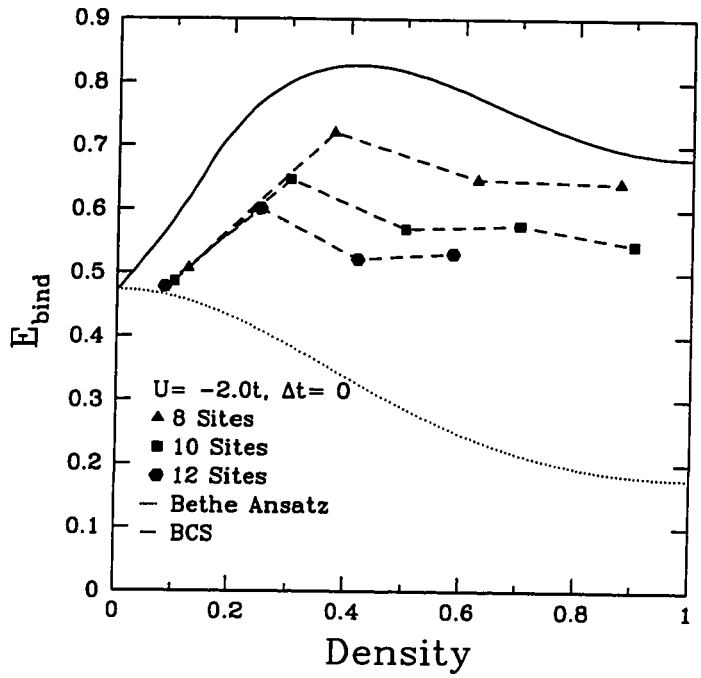

Figure 3.13: Binding Energy for the Attractive Hubbard Model Case $U = -2.0t$

the sign of U being negative in this case. In Figure 3.12 the ground state energy for $U = -2.0t$ is plotted against density for both the BCS and Bethe Ansatz cases [58] along with data for three finite lattices [5]. As can be seen the agreement between the two is excellent for low density while as the density increases a progressive deviation sets in among the two although the correspondence is still good. In fact what is found is that BCS theory very accurately represents the true ground state energy for all densities in the strong and weak coupling regimes. BCS theory disagrees slightly with the exact results for intermediate coupling ranges with the largest deviation on

[5]All BCS data presented in this thesis is taken from Reference [58]. The sharp *kink* in the BCS curves is an artifact of the numerical analysis.

the order of 4 percent at half-filling. All in all then, BCS theory appears to faithfully reproduce the correct energies in 1D in the same way exact diagonalization studies duplicated energies in the repulsive Hubbard model.

As previously noted the solution to the BCS energy gap equations is exact in the low density limit independent of coupling strength. For the attractive Hubbard model Marsiglio found that as the electron density increases the true gap decreases monotonically for all coupling strengths. Furthermore, the BCS gap is found to increase for all coupling strengths as the density increases. The deviation of the BCS gap from the true gap can be seen in Figure 3.13 where the pairing energy is plotted against electron density for the case $U = -2.0t$. This figure demonstrates the significance finite size can have on the gap obtained by exact diagonalization studies. In general it was found that for weak and intermediate coupling strengths the gap increases to a maximum and then decreases while in the strong coupling limit the gap only increases and reaches a maximum at half-filling. For all couplings BCS theory significantly overestimates the magnitude of the gap for all non-zero fillings while in the limit of zero density it is identical to the Bethe Ansatz result and can be given analytically as [57]

$$\Delta = -2t + \sqrt{(\frac{|U|}{2})^2 + (2t)^2}. \tag{3.7}$$

The largest discrepancies are found to occur at half-filling for weak coupling where

the true gap is found to be given by

$$\Delta_{weak}(n=1) = \frac{4}{\pi}\sqrt{|U|t}exp(\frac{-2\pi t}{|U|}) \tag{3.8}$$

and the BCS gap is

$$\Delta^{BCS}_{weak}(n=1) = 8texp(\frac{-2\pi t}{|U|}). \tag{3.9}$$

In strong coupling the dominant terms in the true gap are

$$\Delta_{strong}(n=1) = \frac{|U|}{2} - 2t \tag{3.10}$$

while the strong coupling BCS gap is

$$\Delta^{BCS}_{strong}(n=1) = \frac{|U|}{2} - \frac{2t^2}{|U|}. \tag{3.11}$$

Thus the energy gap, unlike the ground state energy, is not accurately duplicated by BCS theory.

3.8 Finite Size Effects

As many models can only be solved numerically on small systems they are subject to finite size effects. Since the exact solution for this model exists the effects of finite size can be systematically accentuated. The effect of system size on the ground state energy as produced by BCS theory is relatively small compared to the true value. This fact complements earlier discussions which showed that the ground state of the repulsive Hubbard model as given by Bethe Ansatz, is accurately reproduced within exact diagonalization studies on small chains. Furthermore, this fact lends credibility to the ground state energies as derived by exact diagonalization for the Δt model. Within exact diagonalization studies the pair binding energy or charge-transfer gap was calculated as opposed to the spin gap. Finite size effects are found to be more severe in a spin gap calculation. Consider the case of two particles on 16 sites in the attractive Hubbard model with $U = -2.0t$. The spin gap is found to be $0.7855t$ while the pair binding energy is $0.4809t$. For two particles on 32 sites the spin gap is $0.5531t$ and the pair binding is $0.4762t$. Similarly, for 64 sites the spin gap and binding energies are $0.4934t$ and $0.4742t$, respectively. Thus a calculation of the charge gap or pair binding starts to converge much earlier than a similar spin gap calculation. The effect of finite size on the gap was also investigated for both the BCS and Bethe Ansatz approaches. It turns out that finite size effects are prominent only in the weak and intermediate coupling ranges. The overall structure of the BCS gap curves at various finite lattice sizes is qualitatively similar to the bulk case. As the lattice

size approaches the bulk limit the magnitudes of the gap shifts downward. In the exact case for small lattice sizes ($N \leq 16$) the gap is found to display features similar to the BCS results (Figure 3.13). That is, the gap tends to rise first with density then decrease as the density is continuously increased. However as the bulk limit is approached the true gap *only* decreases as a function of increasing carrier concentration. Thus while finite size effects cause the BCS gap to shift downwards slightly with increasing lattice size its overall structure remains the same as the thermodynamic limit is approached. The same conclusions cannot be said for the true gap. Without the bulk result the behaviour of the true gap would not be correctly revealed.
This study futher calls into question the conclusions reached by Hirsch and Lin with regards to the accuracy of BCS theory predictions for the Δt model.

3.9 Re-examination of the Dilute Limit within Exact Diagonalization

The study of Marsiglio further calls into question the conclusions reached by Hirsch and Lin with regards to the accuracy of BCS theory predictions for the Δt model. In particular the initial increase in gap magnitude as a function of hole doping in the low density regime is suspect. The Hubbard Hamiltonian contains no explicit dependence on density and the true gap is found to only decrease with density. Thus, for the Δt model which contains a density dependent *interaction* term, it is not unreasonable to assume that the gap can only decrease with increasing hole density. To investigate this possiblity further, exact diagonalization studies on larger lattices for a dilute

$U = 12.5t,\ \Delta t = 2.0t$

Sites	Density	E(1)	Density	E(3)
8	0.125	1.099	0.375	0.9579
12	0.083	1.075	0.250	1.064
16	0.063	1.111	0.188	1.017
20	0.050	1.105	0.150	1.007
24	0.042	1.101	0.125	1.006
32	0.031	1.073	0.094	1.031
35	0.029	1.072	0.086	1.028
40	0.025	1.073	0.075	1.028
44	0.023	1.073	0.068	1.026
48	0.021	1.088	0.063	1.008
50	0.020	1.088	0.060	1.009
100	0.010	1.073	0.030	—
200	0.005	1.073	0.015	—

Table 3.1: Low Density Exact Diagonalization Studies for $U = 12.5t, \Delta t = 2.0t$.

$U = 6.25t,\ \Delta t = 1.0t$

Sites	Density	E(1)	Density	E(3)
8	0.125	0.4036	0.375	0.3057
12	0.083	0.3572	0.250	0.3927
16	0.063	0.3605	0.188	0.3694
20	0.050	0.3566	0.150	0.3595
24	0.042	0.3546	0.125	0.3518
32	0.031	0.3447	0.094	0.3517
35	0.029	0.3443	0.086	0.3491
40	0.025	0.3447	0.075	0.3469
44	0.023	0.3447	0.068	0.3456
48	0.021	0.3450	0.063	0.3388
50	0.020	0.3497	0.060	0.3386
100	0.010	0.3447	0.030	—
200	0.005	0.3447	0.015	—

Table 3.2: Low Density Exact Diagonalization Studies for $U = 6.25t, \Delta t = 1.0t$.

$U = 10.25t,\ \Delta t = 1.0t$

Sites	Density	E(1)	Density	E(3)
8	0.125	0.0725	0.375	-0.0186
12	0.083	0.0510	0.250	0.0101
16	0.063	0.0487	0.188	0.0208
20	0.050	0.0415	0.150	0.0306
24	0.042	0.0371	0.125	0.0331
32	0.031	0.0286	0.094	0.0385
35	0.029	0.0278	0.086	0.0371
40	0.025	0.0271	0.075	0.0354
44	0.023	0.0267	0.068	0.0342
48	0.021	0.0291	0.063	0.0300
50	0.020	0.0289	0.060	0.0297
100	0.010	0.0260	0.030	—
200	0.005	0.0260	0.015	—

Table 3.3: Low Density Exact Diagonalization Studies for $U = 10.25t, \Delta t = 1.0t$.

density of holes were carried out. The results of this investigation are summarized in Tables 3.1, 3.2, 3.3. The parameters investigated were the same ones used by Hirsch and Lin (Figure 3.11) such that t is normalized to one. The columns show the lattice size investigated followed by the density and energy of the first and then the second pairing point. In strong coupling, Table 3.1, the gap does *not* increase (i.e. $E(1) > E(3)$) as a function of density in agreement with Hirsch and Lin's 12 site case. For intermediate coupling, Table 3.2, the gap starts out decreasing at 8 sites, then increases at 12 sites, then continues to oscillate between increasing and decreasing behaviour. The largest lattice size probed was 50 sites and in this case the gap decreases as a function of density. These results do not support Lin and Hirsch's conjecture that the gap rises for this parameter set. In weak coupling (Table 3.3) at

low lattice sizes (less than 24), the gap decreases with increasing density while for larger lattices it increases slightly. The difference in pairing energy between the first and second density at 50 lattice sites is on the order of $0.001t$. It is feasible that for larger lattices the binding energy will be flat at low denisty and then decrease as a function of increasing hole concentration.

In the next chapter the true gap behaviour of the Δt model will be examined by using a recently developed numerical technique which allows the thermodynamic limit to be probed.

Chapter 4

Real Space Renormalization Group

As previously stated exact diagonalization studies are constrained due to the rapid increase in the dimension of the Hilbert space with increasing lattice size. Moreover, in small lattice systems finite size effects must be systematically studied in order to elucidate and moderate the impact of their behaviour. A recently developed technique called the Density Matrix Renormalization Group [59] (DMRG), makes it possible to study larger lattice sizes and thereby more accurately delimit the thermodynamic or bulk behaviour. In a nutshell, the DMRG process allows larger and larger lattice sizes to be built up iteratively through selective management of the Hilbert space. The DMRG is born out of conventional real space renormalization group techniques and draws its name from these historical roots. The basic idea behind renormalization group is, roughly speaking, a repeated change or redefinition of scale which involves a coarse-graining transformation whereby a system looks like the original system. Renormalization group traditionally has been associated with the process of summing divergent perturbation series but here it is exploited in the context of an iterative

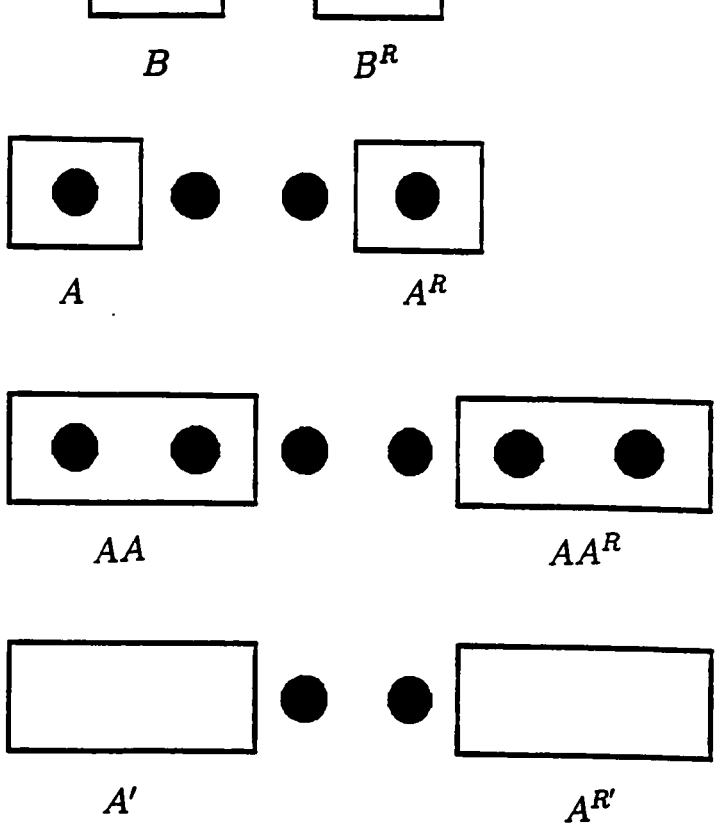

Figure 4.1: Real Space $1D$ Blocking Configuration

numerical diagonalization process.

4.0.1 Conventional Real Space Renormalization Group

The initial architect of the real space renormalization group was Wilson [60]. The basic ideas are presented for 1D systems. However the generalization to higher dimensions utilizes the same algorithm with the treatment of boundary conditions becoming a much more difficult issue [61]. The method will be applied to 1D Hubbard-like Hamiltonians although the technique applies to other lattice models such as the Heisenberg and Kondo model.

The quantum many-body problem is to be solved by first solving a small chain system

and then piecewise building an *infinite* chain. Consider a $1D$ chain as in the top diagram of Figure 4.1 which is broken up into finite identical left and right real space blocks, each labelled B. It is convenient to start with blocks containing just one site. In general block B will contain m basis states so that the Hamiltonian matrix for block B has dimension $m \times m$. The Hamiltonian matrix for the entire chain $\hat{H}_{BB}$ is formed from the block Hamiltonians $\hat{H}_B$ and $\hat{V}_{BB}$ where $\hat{V}_{BB}$ is the matrix representing the interaction between the two blocks. The Hamiltonian matrix for the entire chain is designated as the *superblock*. The dimension of the superblock matrix is given by the product of the sizes of both blocks, that is,

$$dim(\hat{H}_{BB}) = dim(\hat{H}_B) \times dim(\hat{H}_B), \tag{4.1}$$

which in this case would be $m^2 \times m^2$. The interactions in the Hamiltonians under study involve only nearest neighbour sites and the dimension of the interaction matrix is given by the product of the dimension of the left block with the dimension of the right block. In this case since there is only one site in the left and right block $dim(\hat{V}_{BB})$ is equal to that of the superblock matrix. Thus the superblock matrix can be constructed as

$$\hat{H}_{BB} = \hat{H}_B \otimes I^{(1)} + I^{(1)} \otimes \hat{H}_B + \hat{V}_{BB}, \tag{4.2}$$

where $I^{(N)}$ denotes the identity matrix for N sites and in this case it is the identity matrix with the dimensions of a single site. The first term on the right side of the equation represents the *embedding* of the left block in the superblock Hilbert space while the second term denotes the embedding of the right block [1]. The superblock matrix is diagonalized and its lowest lying eigenvalue is the ground state energy for the chain. A new left block Hamiltonian B' which represents the chain BB can be formed from the eigenstates of BB. This block will contain twice as many sites as B. The formal procedure by which this is done is given by

$$\hat{H}_{B'} = \hat{O}\hat{H}_{BB}\hat{O}^{\dagger} \tag{4.3}$$

where $\hat{O}$ is an $n \times m^2$ transformation matrix, the rows of which are n eigenstates of $\hat{H}_{BB}$. If this process were exact the dimension of B' would be equal to that of BB and $\hat{O}$ would be an $m^2 \times m^2$ matrix. Instead only the n lowest lying eigenstates of BB are used so that while B' represents a two site block the dimension of its Hilbert space is *less* than a two site system. In order to form the new interaction matrix between blocks new operator matrices for the block edge sites must also be constructed by applying the above transformation. For example, to form the matrix which represents the hopping of an electron from the edge of the left block to the edge of the right block the transformed matrix operators $\hat{c}'_{left}$ and $\hat{c}^{\dagger\prime}_{right}$ are both required. The superblock Hamiltonian matrix $\hat{H}_{B'B'}$ is now formed and diagonalized

[1] Note the order in which the arguments of the tensor products is placed is important.

as above. This process is continually iterated such that the chain length progressively increases but due to the truncating transformation of Equation 4.3, the dimension of the superblock matrix is kept fixed at a size which can be handled by a computer. This is shown schematically in Figure 4.1. Iteration proceeds until a fixed point has been reached. Typically this means until the ground state energy E_o has converged to a specified accuracy. In keeping the prescribed set of eigenstates, it is assumed that the ground state of larger blocks is well described by the low energy spectrum of the previous block.

Wilson successfully solve the Kondo problem using this prescription. This approach was also used by Bray and Chui [62] to study the eigenstates of the $1D$ Hubbbard model at various fillings. The results they obtained, however, were quite poor and totally unreliable for chains larger than 32 sites. Similarly, Hirsch [63] studied various properties of the $1D$ Hubbard model at half filling and found only qualitative agreement with Bethe Ansatz predictions. At the time, a basis for the inaccuracies in these studies could not be postulated.

4.0.2 The Density Matrix Renormalization Group Technique

It turns out that the above procedure is deficient in the method by which the transformation is handled. Noack and White [64] pointed out that the boundary conditions between the end of the initial left block B and the right block are mismatched. In other words blocks B do not include any connections to the surrounding blocks. In particular, for free fermions the eigenstates of B have nodes on the boundary whereas

the superblock wavefunction ψ_{BB} would have a nonzero amplitude at the boundary between the blocks. In order to remedy this flaw White [59] demonstrated that the optimal set of BB eigenstates to keep is given by the reduced density matrix [2]. One way to see how the Density Matrix Renormalization Group [3] improves upon the conventional approach is to consider a system in contact with a heat reservoir at finite temperature. The probability of the system being in an eigenstate i of the block Hamiltonian is proportional to the Boltzmann weight, $e^{-\beta E_i}$, which is also an eigenvalue of the systems density matrix. Under the assumption that the system is isolated, the lowest energies correspond to the highest probability in Boltzmann weight and in the conventional RG this is consistent with keeping the n most probable eigenstates. Now for a block which is not isolated but strongly coupled to its environment its density matrix is no longer $e^{-\beta H_B}$ (it is defined through Equation 4.8 below.) The eigenstates of the block Hamiltonian no longer share the same set of eigenstates as the density matrix. Consequently for a strongly interacting system rather than use the eigenstates of the system Hamiltonian it is more fitting to utilize the eigenstates of the density matrix to characterize the system.

The construction of the DMRG superblock matrix proceeds analogously to the conventional RG method with a few small changes. It has been found [59, 64] that the most accurate represention of the superblock occurs for open boundary conditions.

[2] See [65] for an excellent discussion on density matrices

[3] Incidentally there are two variations of the DMRG technique, the *infinite* system method and the *finite* system method. This discussion and the calculations carried out in this thesis are for the infinite system method.

That is, a block connects to the rest of the chain only on one end rather than two as in the case of periodic boundary conditions. Additionally, instead of the entire chain potentially doubling in size at each iteration the chain grows by two sites at a time. The DMRG blocking scheme is diagramatically portrayed in Figure 4.1 by the letter A referenced blocks. The left block is designated A while the block on the right is designated A^R where the superscript stands for reflection. Block A^R is the reflection of block A. If block A contained the two sites labelled 1 and 2, then block A^R would have the same cites but inverted as 2 and 1. Placed in between blocks A and A^R are two single sites. The entire lattice or *superblock* can be represented with the notation $A \bullet \bullet A^R$ where $\bullet$ denotes a single lattice site. Typically the block formed from $A\bullet$ is called the *system* while the block $\bullet A^R$ is called the *environment.* The environment serves to mitigate boundary effects that arise from adding a single site to block A. The superblock Hamiltonian matrix $\hat{H}_{super}$ is formed at the first iteration by embedding all the constituent matrices in the superblock Hilbert space

$$\begin{aligned}
\hat{H}_{super} &= \hat{H}^A \otimes I^{(1)} \otimes I^{(1)} \otimes I^{A^R} \\
&+ I^A \otimes \hat{H}^{(\bullet)} \otimes I^{(1)} \otimes I^{A^R} \\
&+ I^A \otimes I^{(1)} \otimes \hat{H}^{(\bullet)} \otimes I^{A^R} \\
&+ I^A \otimes I^{(1)} \otimes I^{(1)} \otimes \hat{H}^{A^R} \\
&+ \hat{H}^{(A\bullet)} \otimes I^{(1)} \otimes I^{A^R} \\
&+ I^A \otimes \hat{H}^{(\bullet\bullet)} \otimes I^{A^R}
\end{aligned}$$

$$+ \quad I^A \otimes I^{(1)} \otimes \hat{H}^{(\bullet A^R)}, \tag{4.4}$$

where I^A is the identity matrix of the dimension of block A, $\hat{H}^{(\bullet)}$ is the Hamiltonain matrix for a single site and $\hat{H}^{(\bullet\bullet)}$ is the matrix representing the interaction between the two single sites.

Now assume that a complete set of states of the system $A\bullet$ is given by

$$|i\rangle, i = 1, \ldots l \ ,$$

while the states of $\bullet A^R$ are

$$|j\rangle, j = 1, \ldots n.$$

Once the superblock is diagonalized its ground state wave function is represented as a direct product of the system's states with those of the environment i.e.

$$|\psi\rangle = \sum_{i,j} \phi_{i,j}(|i\rangle \otimes |j\rangle, \tag{4.5}$$

where the coefficients of $\phi_{i,j}$ are real and $\sum_{i,j} |\phi_{i,j}|^2 = 1$.

Now suppose there are an optimal set of system states $|u^\alpha\rangle, \alpha = 1, \ldots, n$, with $n < l$. That is the states of $A\bullet$ can be approximated accurately by

$$|u^{\alpha}\rangle = \sum_{i} u_{i}^{\alpha} |i\rangle. \tag{4.6}$$

In this case the entire wavefunction of $A \bullet \bullet A^{R}$ can be faithfully re-written as

$$|\psi\rangle \approx |\tilde{\psi}\rangle = \sum_{\alpha,j} a_{\alpha,j} |u^{\alpha}\rangle |j\rangle. \tag{4.7}$$

White examined the minimization problem

$$||\psi\rangle - |\tilde{\psi}\rangle|^{2},$$

subject to the constraint $\langle u^{\alpha}|u^{\alpha'}\rangle = \delta_{\alpha,\alpha'}$ and varying over all $a_{\alpha,j}$. White found the solution to this problem is given by the optimal set of states $|u^{\alpha}\rangle$ being the eigenvectors of the *reduced* density matrix of the system as part of the superblock whose eigenvalues are largest in magnitude. The *reduced density matrix* depends on the state of the superblock $|\psi\rangle$ and is formed from the following construction

$$\rho_{i,i'}^{red.} = \sum_{j} \phi_{i,j} \phi_{i',j}. \tag{4.8}$$

The eigenvalues of $\hat{\rho}^{red.}$, a_{α} represent the probability of the system being in the state v_{α} with

$$\sum_{\alpha} a_{\alpha} = 1. \tag{4.9}$$

The eigenvectors of the reduced density matrix v_{α} form the rows of the transformation matrix $\hat{O}$ in Equation 4.3 and each eigenvector represents *one* basis state in the *new* truncated basis. Only n eigenvectors with the largest weights a_{α} will be kept and the accuracy of the truncation is measured by the deviation of the sum

$$D_n = \sum_{\alpha=1}^{n} a_{\alpha} \tag{4.10}$$

from unity. All the eigenvalues and eigenvectors of $\hat{\rho}^{red.}$ are required so that a *dense* matrix diagonalization routine must be used [4].

As in conventional RG in order to construct the superblock at the next iteration information describing the interactions between blocks is also needed. Once these operators are formed, Equation 4.3 is used to produce the interaction matrix $\hat{H}^{(A'\bullet)}$ between block A' and a new single lattice site.

The above procedure is iterated until convergence is achieved as in the RG process. The DMRG algorithm is summarized in Appendix 1.

n	L	N1	N2	w1	w2
0.60	4	2	3	0.6	0.4
0.60	6	3	4	0.4	0.6
0.60	8	4	5	0.2	0.8
0.60	10	6	—	1.0	—
0.60	12	7	8	0.8	0.2
0.60	14	8	9	0.60	0.4
⋮	⋮	⋮	⋮	⋮	⋮

Table 4.1: Sample Table of Parameter Values for Targetting Procedure in DMRG

4.0.3 Arbitrary Band Filling

The particle density n for a fixed chain length L is defined in terms of the total number of fermions as

$$n = \frac{N\uparrow + N\downarrow}{L} \tag{4.11}$$

where $N\uparrow$ ($N\downarrow$) represent the number of spin-up (down) particles present. As the number of $N\uparrow$ and $N\downarrow$ particles must be integers it is difficult to choose them so that an arbitrary number density remains constant on different lattice sizes. In fact, as the chain length is even in the total number of sites at each iteration, only the half-filling ($n = 1.0$) and quarter filling ($n = 0.5$) densities remain invariant at each iteration. To remedy this problem one can target one or more states closest to the proper density [66]. Specifically two nearest integers N_1 and N_2 can be found such

[4]See reference [46] for example.

that

$$N_1 \leq nL \leq N_2. \tag{4.12}$$

Now the reduced density matrix can be constructed from the two ground states that bracket the required density n. Specifically if the ground state wave function for N_1 particles is $|\psi(N_1)\rangle$ and that for N_2 particles is $|\psi(N_2)\rangle$ then the following construction is engaged

$$\begin{aligned} \rho^{red.}_{i,i'} &= w_1 \sum_j \phi_{i,j}(N_1)\phi^*_{i',j}(N_1) + w_2 \sum_j \phi_{i,j}(N_2)\phi^*_{i',j}(N_2) \\ nL &= w_1 N_1 + w_2 N_2 \\ 1 &= w_1 + w_2. \end{aligned} \tag{4.13}$$

The equations in 4.13 ensure that the proper particle filling is targetted at each iteration. If N_1 or N_2 is odd, then the corresponding ground state wave function is two fold degenerate as either total spin $\uparrow$ or total spin $\downarrow$ is possible. In this case both states are used in the targetting process. In Table 4.1 a typical sample of parameters is given for a target density of $n = 0.60$ as the lattice size grows. At a lattice size of 8 sites the ground state wavefunction for occupations of 4 and 5 particles must be calculated. Appropriate weights of these wavefunctions are then used to calculate the reduced density matrix.

4.0.4 Algorithm Implementation Tips

In all cases it is extremely important to utilize the fact that the reduced density matrix and superblock Hamiltonian are block diagonal. The eigenvectors of the reduced density matrix could be incorrectly produced otherwise thereby yielding an incorrect transformation matrix. Eigenvectors of distinct eigenvalues are orthogonal whereas for degenerate eigenvalues this may not necessarily be the case. Thus the reduced density matrix must be block diagonalized to avoid complications that could arise due to eigenvalue degeneracies in different quantum number sectors. Additionally, a matrix which is block diagonal can be diagonalized block by block which is less CPU intensive than diagonalizing the entire matrix at once. For the superblock Hamiltonian only the block which contains the number of particles specific to the density being probed is required.

4.0.5 Accuracy

The DMRG routine is a *value added* algorithm in that parameters must be carefully optimized in order to attain acceptable results. The quality of the results hinges upon how accurate the approximation in Equation 4.7 is. That is, accuracy of convergence depends strongly on the number of states kept in the truncation procedure. In Figure 4.2 the reduced density matrix eigenvalues a_α are plotted against eigenvalue index α for a 100 site repulsive Hubbard system at half-filling and $U = 4.0t$. The number of states kept in this case is chosen to be constant at 110. To appreciate what this means consider the *zeroeth iteration* or the beginning of a DMRG process. If block B

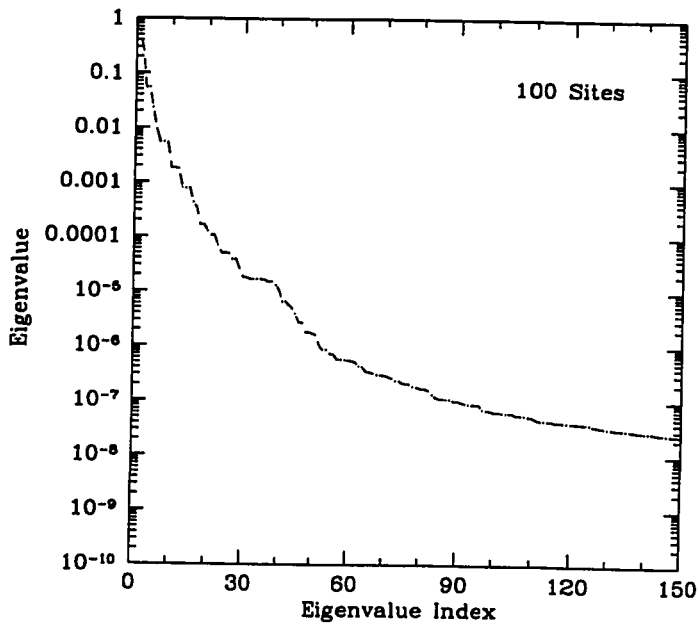

Figure 4.2: Reduced Density Matrix Eigenvalue versus Eigenvalue Index for a 100 Site Chain

is initially chosen to contain 3 sites the entire length of the initial superblock chain is $3+1+1+3$ or 8 sites. The dimension of the superblock matrix is then $4^8 \times 4^8$ while the reduced density matrix (for the $3+1$ site block) is of order $4^4 \times 4^4$. Thus there will be 256 eigenvalues from which 110 eigenvectors with the largest eigenvalues are chosen to construct the transformation matrix $\hat{O}$. The truncated block B' at the next iteration is then of dimension 110×110 making superblock Hamiltonian matrix of dimension $440^2 \times 440^2$ [5]. The reduced density matrix in this case (and every subsequent iteration) will contain 440 eigenvalues from which the 110 largest are kept. As previously mentioned the partial sum of the eigenvalues retained relates

[5]Recall that the matrix is block diagonal so that the actual size of the matrix to be diagonalized is much smaller than this very large dimension.

to the accuarcy of the truncation. For this example Figure 4.2 shows that by keeping 110 eigenvalues when the lattice size is 100 sites the accuracy of the truncation is on the order of 10^{-7}. If the DMRG is repeated for the same set of parameters but only 70 states are kept at each iteration accuracy of the approximation drops to about 10^{-3}. It must be stressed that the sum of the eigenvalues retained is *only a useful indicator of the accuracy of the calculation.* A smaller sum indicates that a result is less accurate than a larger sum. In the above example where 110 and 70 states are kept, the ground state energy per site is found to be $-0.57366t$ and $-0.57243t$, respectively. The exact result from Bethe Ansatz is $-0.57373t$. The 110 state case is *not* accurate to within $10^{-7}t$ of the Bethe Ansatz result. Incidentally, the step-like structure in Figure 4.2 comes from the presence of spin degeneracies.

Another factor that has a direct bearing on the accuracy of DMRG ground state energies is is the coupling strength. For the repulsive Hubbard model the DMRG is least accurate for $U = 0$ while the accuracy is best for large values of U. One can anticipate this fact as a system which is free particle-like requires many more local basis states to describe it than would a system where large correlations restrict (and thereby reduce) possible particle configurations.

As already mentioned the DMRG is most accurate at half-filling while away from half-filling the *targetting* of particle occupations that bracket the desired density reduces the accuracy. A measure of DMRG accuracy in this case can be realized by examining the energy difference between a chain of length L with N and $N-1$ particles. For

the repulsive Hubbard model this difference should be equal to the coupling U. At $U = 2.0t$ and $n = 0.10$ this difference is equal to the Hubbard U to an accuracy of about 10^{-3}.

In Chapter 3 it was pointed out that of the two possible methods by which the energy gap can be calculated, the charge gap calculation is influenced by finite size effects to a lesser degree than the spin gap. Consequently all DMRG pairing energies are determined via the binding energy or charge gap method. In the context of a DMRG calculation this means that in order to calculate one binding energy the ground state energy at three different particle occupations (or densities) is required. If however, the corresponding spin gap is to be calculated the ground state energy at only *one* targetted density is required. In calculating the spin gap at a particular density the ground state energy of the zero spin and spin-one sectors are obtained from the single superblock matrix. This means only one run of the DMRG algorithm is required versus three in the charge gap case where the ground state energy for the zero spin sector at three densities is needed. Thus to minimize computer run time a spin gap calculation would appear more beneficial than a charge gap calculation. The rates of convergence in this scenario need to be compared before it can be definitely concluded that the spin gap method is optimal.

4.1 Results

The intent of using the DMRG is to numerically *expose* the thermodynamic behaviour of models for which an exact solution is lacking. In this thesis the model under study

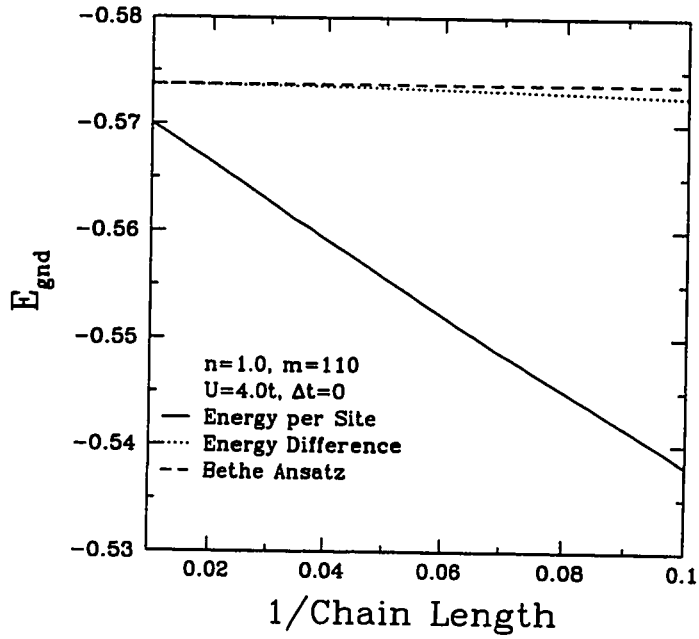

Figure 4.3: Comparison of the Convergence of the Ground State Energy with Lattice Size.

is the Δt model while exact results from the Hubbard model are used to benchmark the correct operation of the numerical routines. In particular the DMRG is used as a check on those results obtained from the exact diagonalization of finite chains and to characterize the quality of the BCS approximation.

In discussing the exact diagonalization ground state energies for the Δt model it was pointed out that for finite lattices there are actually two paths of convergence for the ground state energy. One path is based on odd particle occupations and the other is for even. Keeping this in mind, the best way to extract the ground state energy per site is to take the difference in energy between superblocks which differ in size

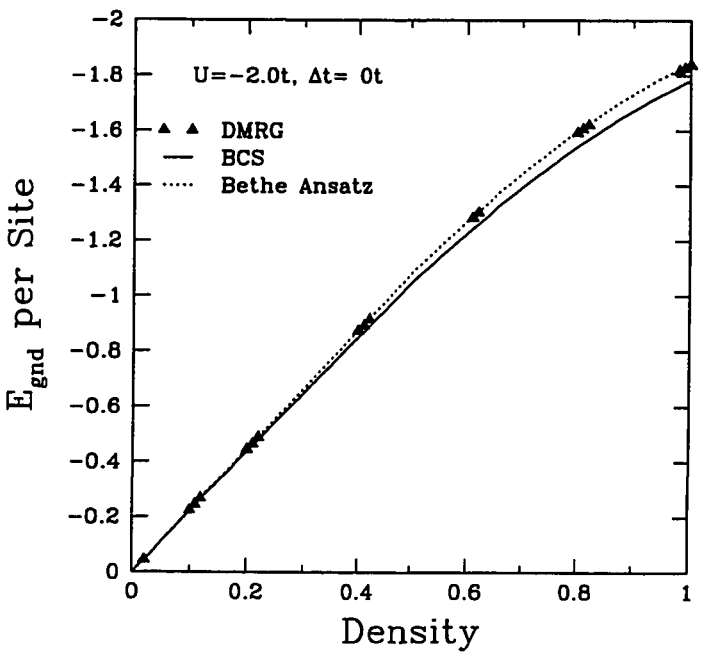

Figure 4.4: Comparison of the DMRG, BCS and Bethe Ansatz Ground State Energies for the Attractive Hubbard Model Case $U = -2.0t$.

by four sites and then divide by four. Steps of four are chosen because superblock sizes in multiples of four follow the same path of energy convergence. Additionally, this method helps to reduce the effect of finite sizes. In Figure 4.3 the convergence of energy with increasing lattice size at half-filling is shown for the repulsive Hubbard model. The horizontal dashed line is the Bethe Ansatz ground state energy while the dotted line shows the DMRG convergence of energy as obtained by the above energy difference method while the solid line is just the DMRG energy at a specific lattice size divided by that size. This plot shows that the difference method converges much faster and accurately to the exact result.

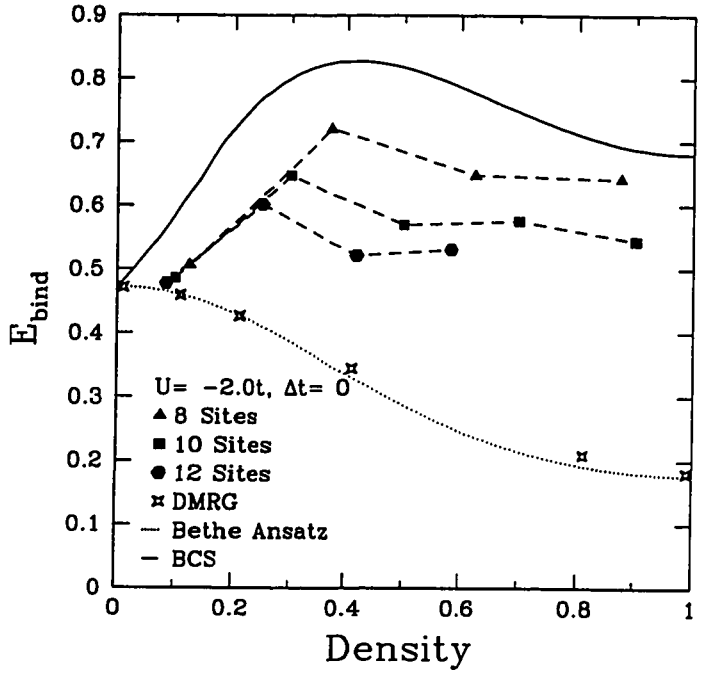

Figure 4.5: Comparison of the Binding Energies obtained in Exact Diagonalization, DMRG, BCS, and Bethe Ansatz Studies for the Attractive Hubbard Model Case $U = -2.0t$.

The DMRG ground state energies for densities away from half-filling is benchmarked against BCS and Bethe Ansatz results for the attractive Hubbard model in Figure 4.4. The DMRG results are in excellent agreement with Bethe Ansatz predictions while the BCS energies tend to underestimate the exact energy as the density increases. The pair binding energies for the above techniques and for those obtained by Exact Diagonalization are plotted in Figure 4.5. The DMRG and Bethe Ansatz gap are in good agreement while the BCS and Exact Diagonalization outcomes tend to agree with one another but not with the true results. The fact that the DMRG results

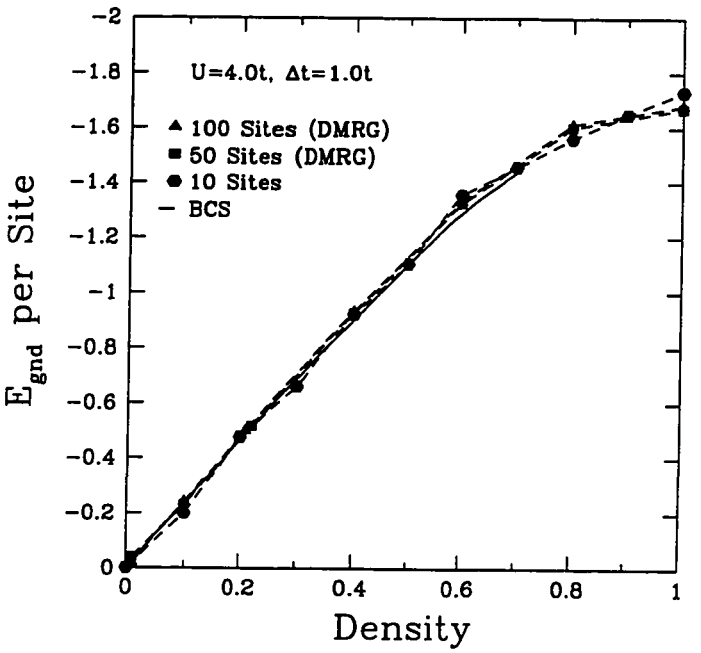

Figure 4.6: Comparison of the DMRG, BCS and Exact Diagonalization Ground State Energies for the Δt Model.

corroborate the true properties of the gap in this model (as well as the ground state energies) points out its significance as a numerical technique able to reveal thermodynamic behaviour. With this in mind, the Δt model Exact Diagonalization and BCS results of Chapter 3 can now be cross-examined.

In Figure 4.6 the ground state energy is plotted against density in the Δt model for $U = 4.0t$ and $\Delta t = 1.0t$. DMRG results for 50 and 100 sites are shown along with BCS results and exact diagonalization results for a 10 site chain. In all cases the correspondence between energies is good. The data points for the 50 and 100 site energies coincide for the most part indicating that the energies have converged to the

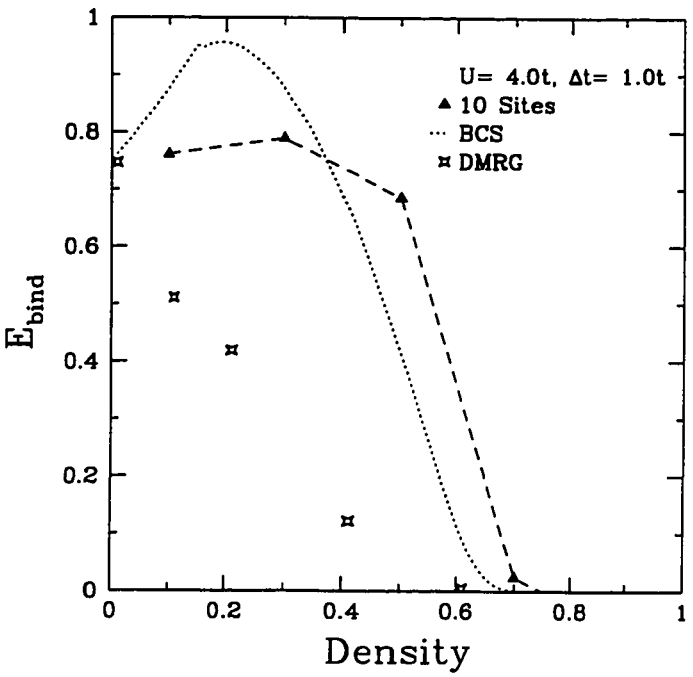

Figure 4.7: Comparison of the DMRG, BCS and Exact Diagonalization Pair Binding Energies for the Δt Model.

bulk limit. The 10 site case deviates slightly from the larger lattices particularly at higher densities where correlations are strongest. The agreement of energies is not unexpected as there has been little indication of discrepancies in all of the methods presented so far. The gap or pair binding energy has been a different matter.

The pair binding energies corresponding to the energies of the above techniques are plotted in Figure 4.7. The DMRG data at the densities probed is shown as open symbols, solid symbols represent Exact Diagonalization data and the dotted line is Marsiglio's BCS data. For this parameter set the DMRG gap is a decreasing function of increasing density unlike the BCS and Exact Diagonalization plots. This data

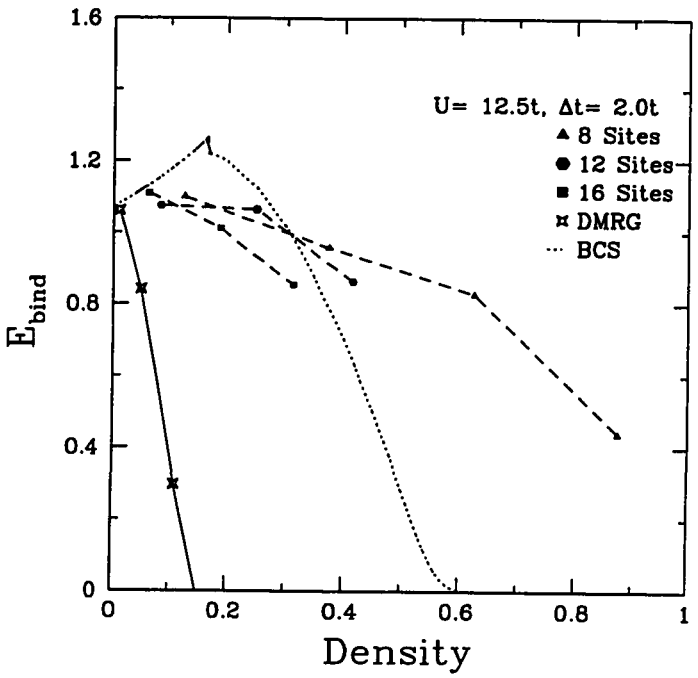

Figure 4.8: DMRG, BCS and Exact Diagonalization Pair Binding Energies for $U = 12.5t, \Delta t = 2.0t$.

suggests that within Exact Diagonalization studies finite size effects are too significant for the lattice sizes that can be investigated. Moreover, these results show that BCS theory does not provide an adequate description of gap behaviour in the low density limit but rather only in the *zero* density limit. This outcome reinforces suspicions raised at the end of Chapter 3 as to the true gap behaviour in the Δt model as claimed by Hirsch and Lin.

In Figure 4.8 DMRG results are shown for the parameters $U = 12.5t$ and $\Delta t = 2.0t$. Also presented are the corresponding results as obtained within BCS and Exact Diagonalization studies. Hirsch and Lin's Exact Diagonalization results (Figure 3.11)

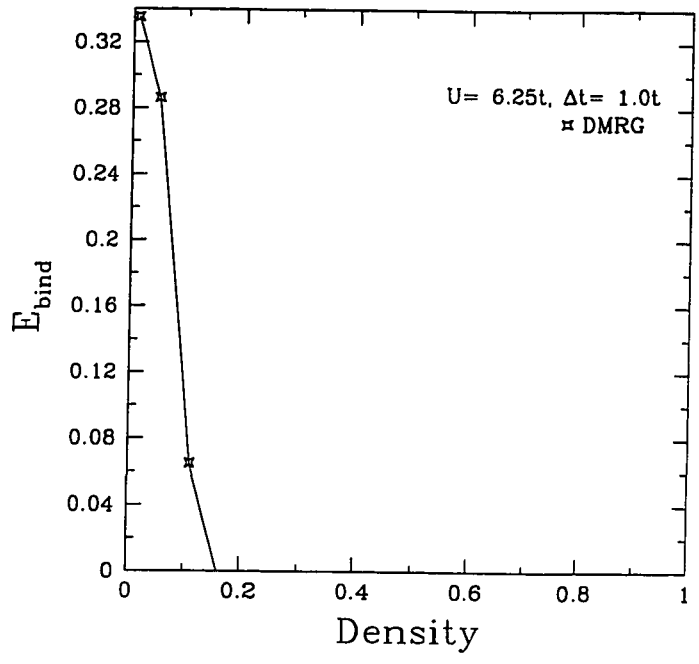

Figure 4.9: DMRG Binding Energy Data for $U = 6.25t, \Delta t = 1.0t$.

for these parameters show the gap to be flat at low density rather than increasing as in the BCS case. The DMRG data in Figure 4.8 clearly show the gap to be a decreasing function of density which could have a flat edge near zero density. For these parameters the range over which there is pairing in the DMRG case is significantly reduced from the BCS result. Figure 4.9 shows the DMRG binding energy versus density for the weaker coupling case of $U = 6.25t$ and $\Delta t = 1.0t$. Once again the gap shows no indication of the behaviour predicted by BCS theory. Hirsch and Lin show the gap rising slightly in their Exact Diagonalization results on a 12 site chain. In Chapter 3 low density Exact Diagonalization studies on chains up to 50 sites (Table 3.2) hinted that finite size effects are too significant in the 12 site chain to

conclude that the true behaviour of the gap is well-produced by BCS theory. The DMRG data justifies the conclusion that the gap behaviour does *not* conform to BCS predictions which is contrary to the conclusions of [52].

Chapter 5

Conclusions

In this thesis the DMRG routine has been exploited to calculate the ground state energy and pair binding energy of the Δt model in 1D. In doing so the BCS theory predictions for this model as put forth by other authors have been evaluated. Additionally, the effect of finite size on small cluster studies has been investigated. The ground state energy as calculated within BCS, Exact Diagonalization, and DMRG studies is found to compare favourably in all cases. Agreement at all coupling strengths is best at low particle densities while the greatest deviation, which is still small, occurs at half-filling. In the attractive Hubbard model the DMRG ground state energy agrees with the Bethe Ansatz results even better than BCS predictions do. This agreement reinforces the worthwhileness of the DMRG as a numerical technique capable of soliciting thermodynamic or bulk behaviour.

The results for the energy gap or pair binding are not as synonymous. As found in the attractive Hubbard model, the Δt model BCS gap behaviour is contrary to the results obtained with the DMRG. This result is antithetical to the conclusions reached in

other parallel studies. BCS theory does *not* in general provide a reliable description of the exact gap behaviour in 1D. Finite size effects in Exact Diagonalization studies on small clusters are robust enough to mask true gap behaviour. This is especially true for weak coupling parameters. Only in the limit of zero density is there direct agreement between BCS theory and exact results. Whether or not this conclusion carries over to higher dimensions remains an open question.

To reduce the time required to extract pairing energies from the DMRG it is recommended that a detailed comparison between spin gap and charge gap calculations be carried out. By further optimizing the routine speed a larger range of densities can be probed thereby permitting the gap behaviour to be mapped out in greater detail particularly at low densities.

On the basis of the results presented in this thesis it is the author's opinion that the use of BCS results (by others) to advocate the relevancy of the Δt model in describing High Temperature Superconductors is suspect.

Appendix A

1D DMRG Algorithm

1. Make 4 initial blocks where the first (left) block contains 1 or more sites*, the 'second' and 'third blocks' consist of a single site and the fourth (right) block is a spatial reflection of the 1^{st} block (Figure 4.1).

2. Form the (sparse) Hamiltonian matrix $\hat{H}^{superblock}$ for the superblock.

3. Diagonalize $\hat{H}^{superblock}$ using a Lanczos routine to obtain the ground state wave function ψ.

4. Form the reduced density matrix $\hat{\rho}^{red.}$ for the block system 1+2 using Equation.

5. Diagonalize $\hat{\rho}^{red.}$ to obtain all the eigenvectors v_α and eigenvalues a_α and discard all but the largest m eigenvalues and corresponding eigenvectors.

6. Form matrix representations for active spin operators (those on the ends) of the two block system.

7. Generate new block 1 by changing basis to the v_α using Equation 4.3. Transform operators in 6.) using the same equation.

8. Replace old block 1 with new block 1 and old block 4 with the reflection of new block 1.

9. Repeat at step 2.) until convergence is obtained.

Bibliography

[1] D. Bohm and F. David Peat, *Science, Order, and Creativity*, Bantam Books, Toronto, 1987, p. 8.

[2] H. K. Onnes, *Comm. Leiden* **120b**, (1911).

[3] J. Bardeen, L. N. Cooper, and J. R. Schrieffer, *Phys. Rev.* **108**, 1175 (1957).

[4] G. M. Eliashberg, *Zh. Eksperim. i Teor. Fiz.* **38**, 966 (1960); *Soviet Phys. JETP* **11**, 696 (1960).

[5] M. A. Preston and R. K. Bhaduri, *Structure of the Nucleus*, Addison-Wesley, Readsin, MA, 1975.

[6] J. G. Bednorz and K. A. Müller, *Z. Phys.* **B64**, 189 (1986).

[7] L. N. Cooper, *Phys. Rev.* **104**, 1189 (1956).

[8] E. Maxwell, *Phys. Rev.* **78**, 477 (1950).

[9] C. A. Reynolds, B. Serin, W. H. Wright, and L. B. Nesbitt, *Phys. Rev.* **78**, 487 (1950).

[10] H. Fröhlich, *Phys. Rev.* **79**, 845 (1950).

[11] G. Rickayzen, *Theory of Superconductivity*, Wiley and Sons, New York, 1965.

[12] J. R. Schrieffer, *Theory of Superconductivity*, Benjamin/Cummings, Don Mills, 1964.

[13] D. Pines and P. Nozières, *The Theory of Quantum Liquids: Normal Fermi Liquids*, Addison-Wesley, Don Mills, 1989.

[14] Shen et al., *J. Phys. Chem. Solids* **54**, 1169 (1993).

[15] A. G. Loeser, Z.-X. Shen, and D. S. Dessau, *Physica* **C263**, 208 (1996).

[16] D. A. Wollman, D. J. Van Harlingen, W. C. Lee, D. M. Ginsberg, and A. J. Leggett, *Phys. Rev. Lett.* , **71**, 2134 (1993).

[17] N. W. Ashcroft and N. D. Mermin, *Solid State Physics*, Saunders College, Holt, Rinehart, and Winston, Philadelphia, 1976.

[18] B. G. Levi, *Phys. Today*, June 1996, pp. 17-19.

[19] W. Heitler and F. London, *Z. Phys.* **44**, 455 (1927).

[20] D. R. Hartree, *Proc. Cambridge Philos. Soc.* , **24**, 89 (1928); V. Fock, *Z. Phys.* , **61**, 126 (1930); J. C. Slater, *Phys. Rev.* , **35**, 210 (1930).

[21] J. Hubbard, *Proc. Roy. Soc. London, Ser. A* , **276**, 238 (1963); **277**, 237 (1964); **281**, 401 (1964).

[22] M. Schluter and M. Hybertsen, *Physica* **C162-164**, 583 (1989).

[23] V. J. Emery, *Phys. Rev. Lett.* **58**, 2794 (1987).

[24] E. H. Lieb and F. Y. Wu, *Phys. Rev. Lett.* **20**, 1445 (1967).

[25] W. Metzner and D. Vollhardt, *Phys. Rev. Lett.* **62**, 324 (1989); M. Jarrell, *Phys. Rev. Lett.* **69**, 168 (1992).

[26] F. C. Zhang and T. M. Rice, *Phys. Rev.* **B37**, 3759 (1988).

[27] J. E. Hirsch, *Physica* **C158**, 326 (1989).

[28] E, Fradkin, *Field Theories of Condensed Matter Systems*, Addison-Wesley, Reading, MA, 1991.

[29] H. Bethe, *Z. Phys.* **71**, 205 (1931).

[30] B. Sutherland, in *Exactly Solvable Problems in Condensed Matter and Relativistic Field Theory*, edited by B. S. Shastry, S. S. Jha, and V. Singh, Springer-verlag, Berlin, p.1 ,1985.

[31] L. H. Lieb and F. Y. Wu, *Phys. Rev.* **125**, 164 (1962).

[32] Landau and Lifshitz, *Statistical Physics*, Pergamon Press, London, 1980.

[33] H. Shiba, *Phys. Rev.* **B6**, 930 (1972).

[34] P. Anderson, *Science* **235**, 1196 (1987).

[35] H. Eskes, B. J. Meinders, and G. A. Sawatzky, *Phys. Rev. Lett.* **67**, 1035 (1991); B. J. Meinders, H. Eskes, and G. A. Sawatzky, *Phys. Rev.* **B48**, 3916 (1993).

[36] D. B. Tanner, Y.-D. Yoon, A. Zibold, H. L. Liu, M. A. Quijada, S. W. Moore, J. B. Graybeal, Beom-Hoan O., J. T. Markert, R. J. Kelley, M. Onellion, and J. -H. Cho, *preprint.*

[37] J. E. Hirsch, *Physica* **B199-200**, 366 (1994).

[38] J. E. Hirsch, *Phys. Rev.* **B48**, 3327 (1993).

[39] H. Hotop and W. C. Lineberger, *J. Phys. Chem. Ref. Data* **4**, 539 (1975).

[40] O. Gunnarson and N. E, Christensen, *Phys. Rev.* **B42**, 2363 (1990); M. S. Hybertsen, E. B. Stechel, and D. R. Jennsion, *Phys. Rev.* **B41**, 11068 (1990).

[41] F. Marsiglio and J. Hirsch, *Phys. Rev.* **B41**, 6435 (1990); *Phys. Rev.* **B39**, 11515 (1989).

[42] J. Hirsch, *Physica* **C158**, 326 (1989).

[43] S. Chakravarty, A. Sudbo, P. W. Anderson, and S. Strong, *Science* **261**, 337 (1993).

[44] F. Marsiglio and J. Hirsch, *Physica* **C171**, 554 (1990).

[45] I. M. Chapnik, *Dok. Akad. Nauk SSSR* **141**, 70 (1960) [*Sov. Phys. Dokl.* **6**, 988 (1962)]; *J. Phys.* **F13**, 975 (1983).

[46] "Numerical Recipes': The Art of Scientific Computing", by W. H. Press, B. P. Flannery, S. A. Teukolsky, and W. T. Vetterling, Cambridge University Press. Cambridge, 1986.

[47] H. Q. Lin and J. E. Gubernatis, *Comput. Phys.* **7**, 400 (1993).

[48] E. Dagotto, *Rev. Mod. Phys.* **66**, 763 (1994).

[49] J. A. Riera and A. P. Young, *Phys. Rev.* **B39**, 9697 (1989).

[50] R. M. Fye, M. J. Martins, and R. T. Scalettar, *Phys. Rev.* **B42**, 6809, (1990).

[51] P. Nozières and S. Schmitt-Rink, *J. Low Temp. Phys.* **59**, 195 (1985).

[52] H. Q. Lin and J. E. Hirsch, *Phys. Rev.* **B52**, 16155 (1995).

[53] M. Quaisser, A. Schadschneider, and J. Zittartz, *Europhys. Lett.* **32**, 179 (1995).

[54] R. Bariev, *J. Phys.* **A24**, L549 (1991).

[55] L. Arrachea, A. A. Aligia, E. Gagliano, K. Hallberg, and C. Balseiro, *Phys. Rev.* **B50**, 16044 (1994).

[56] M. Airoldi and A. Parola, *Phys. Rev.* **B51**, 16327 (1995).

[57] F. Marsiglio, *Phys. Rev.* **B**, (Jan. 1997).

[58] F. Marsiglio, *Private communication.*

[59] S. R. White, *Phys. Rev. Lett.* **69**, 2863 (1992); *Phys. Rev.* **B48**, 10345 (1993).

[60] K. G. Wilson, Rev. Mod. Phys. **47**, 773 (1975).

[61] S. Liang and H. Pang, *Phys. Rev.* **B49**, 9214 (1994).

[62] J. W. Bray and S. T. Chui, *Phys. Rev.* **B18**, 2426 (1978); *Phys. Rev.* **B19**, 4876 (1979).

[63] J. E. Hirsch, *Phys. Rev.* **B22**, 5259 (1980).

[64] S. R. White and R. M. Noack, *Phys. Rev. Lett.* **68**, 3487 (1992).

[65] R. P. Feynman, *Statistical Mechanics: A set of Lectures*, Benjamin, Reading, MA, 1972.

[66] L. Chen and S. Moukouri, *Phys. Rev.* **B53**, 1866 (1996).

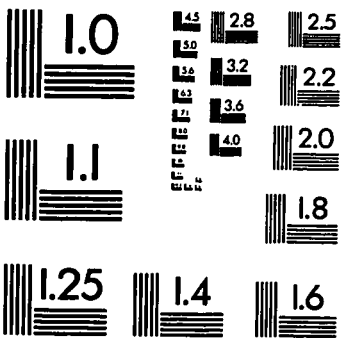

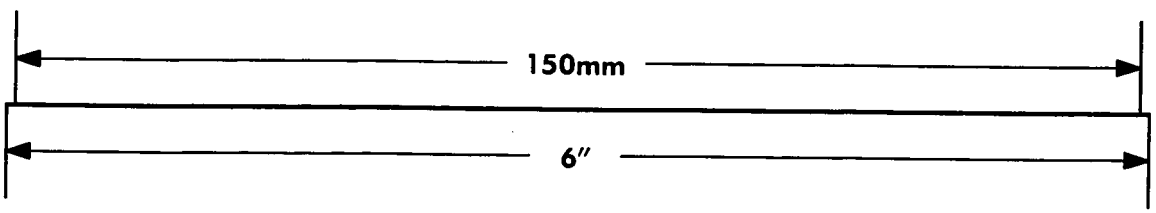

APPLIED IMAGE, Inc
1653 East Main Street
Rochester, NY 14609 USA
Phone: 716/482-0300
Fax: 716/288-5989